Table I. Continued

genes	foldchange	t-test p-value
transcription		
Cardiac-specific homeo box	2.095	0.170
wa17f11.x1 NCI_CGAP_Kid11 Homo sapiens cDNA clone IMAGE:2298381 3' similar to TR:Q15886 Q15886 X-LINKED NUCLEAR PROTEIN ;, mRNA sequence.	2.435	0.276
Cofactor required for Sp1 transcriptional activation, subunit 3 (130kD)	2.376	0.132
Wolf-Hirschhorn syndrome candidate 1-like 1	2.047	0.013
cell proliferation		
Tumor necrosis factor receptor superfamily, member 9	2.651	0.084
Interleukin 1, beta	2.233	0.001
Interleukin 1, alpha	2.150	0.019
Interleukin 12A (natural killer cell stimulatory factor 1, cytotoxic lymphocyte maturation factor 1, p35)	2.124	0.162
Epidermal growth factor receptor (avian erythroblastic leukemia viral (v-erb-b) oncogene homolog)	2.093	0.066
nad20g10.x1 NCI_CGAP_Lu24 Homo sapiens cDNA clone IMAGE:3366330 3', mRNA sequence.	2.031	0.087
transport		
Solute carrier family 4, sodium bicarbonate cotransporter-like, member 10	3.528	0.166
UI-H-BW0-ajo-f-12-0-UI.s1 NCI_CGAP_Sub6 Homo sapiens cDNA clone IMAGE:2732686 3', mRNA sequence.	2.468	0.423
Solute carrier family 35 (UDP-N-acetylglucosamine (UDP-GlcNAc) transporter), member 3	2.110	0.152
Solute carrier family 21 (organic anion transporter), member 3	2.031	0.030

Table II. Fold changes of specific genes in T24 cells treated with BCH for 12 h

gene	foldchange	t-test p-value
enzyme		
GDP-mannose pyrophosphorylase B	0.306	0.078
AU121975 MAMMA1 Homo sapiens cDNA clone MAMMA1001393 5', mRNA sequence.	0.319	0.235
Polymerase (DNA directed), mu	0.334	0.159
Adenylate kinase 2	0.353	0.015
F-box only protein 9	0.362	0.057
Stearoyl-CoA desaturase (delta-9-desaturase)	0.362	0.046
N-myristoyltransferase 1	0.370	0.095
Protein phosphatase 2 (formerly 2A), regulatory subunit B" (PR 72), alpha isoform and (PR 130), beta isoform	0.383	0.078
Homo sapiens Scd mRNA for stearoyl-CoA desaturase, complete cds.	0.384	0.009
qd05f07.x1 Soares_placenta_8to9weeks_2NbHP8to9W Homo sapiens cDNA clone IMAGE:1722853 3' similar to SW:ER19_HUMAN P53602 DIPHOSPHOMEVALONATE DECARBOXYLASE ;contains MER22.b1 MSR1 repetitive element ;, mRNA sequence.	0.404	0.013
602022620F1 NCI_CGAP_Brn67 Homo sapiens cDNA clone IMAGE:4158005 5', mRNA sequence.	0.406	0.020
N-acetylglucosaminidase, alpha- (Sanfilippo disease IIIB)	0.407	0.279
3-hydroxybutyrate dehydrogenase (heart, mitochondrial)	0.409	0.238
Creatine kinase, mitochondrial 2 (sarcomeric)	0.440	0.135
Phosphodiesterase 4D, cAMP-specific (dunce (Drosophila)-homolog phosphodiesterase E3)	0.441	0.020
qi08f09.x1 Soares_NhHMPu_S1 Homo sapiens cDNA clone IMAGE:1855913 3', mRNA sequence.	0.454	0.071
AL525798 LTI_NFL003_NBC3 Homo sapiens cDNA clone CS0DC013YB08 5 prime, mRNA sequence.	0.454	0.020
KIAA0015 gene product	0.455	0.043
Glutaryl-Coenzyme A dehydrogenase	0.467	0.082
Polynucleotide kinase 3'-phosphatase	0.470	0.079
Enolase 2, (gamma, neuronal)	0.471	0.008
xn86c10.x1 Soares_NFL_T_GBC_S1 Homo sapiens cDNA clone IMAGE:2701362 3' similar to TR:Q99766 Q99766 HYPOTHETICAL 15.7 KD PROTEIN. ; mRNA sequence.	0.481	0.112

Table II. Continued

gene	foldchange	t-test p-value
enzyme		
Serine hydroxymethyltransferase 1 (soluble)	0.483	0.092
Crystallin, zeta (quinone reductase)-like 1	0.486	0.042
xd94e03.x1 Soares_NFL_T_GBC_S1 Homo sapiens cDNA clone IMAGE:2605276 3' similar to WP:Y116A8C.27 CE23335 ;, mRNA sequence.	0.488	0.213
Aminoacylase 1	0.488	0.016
H.sapiens pseudogene for mitochondrial ATP synthase c subunit (P2 form).	0.491	0.088
zi27a06.s1 Soares_fetal_liver_spleen_1NFLS_S1 Homo sapiens cDNA clone IMAGE:431986 3', mRNA sequence.	0.491	0.061
Fatty-acid-Coenzyme A ligase, long-chain 3	0.492	0.069
Triosephosphate isomerase 1	0.494	0.322
Tumor necrosis factor receptor superfamily, member 6b, decoy	0.495	0.000
transcription		
Paired box gene 3 (Waardenburg syndrome 1)	0.342	0.260
Paired box gene 8	0.423	0.218
AU118165 HEMBA1 Homo sapiens cDNA clone HEMBA1003008 5', mRNA sequence.	0.466	0.057
Core promoter element binding protein	0.447	0.016
Death effector domain-containing	0.484	0.028
Trinucleotide repeat containing 11 (THR-associated protein, 230 kDa subunit)	0.498	0.002
NS1-binding protein	0.335	0.018
Hypothetical protein	0.484	0.031
602437464F1 NIH_MGC_46 Homo sapiens cDNA clone IMAGE:4555622 5', mRNA sequence.	0.486	0.027
601872674F1 NIH_MGC_54 Homo sapiens cDNA clone IMAGE:4096483 5', mRNA sequence.	0.432	0.002
Cofactor required for Sp1 transcriptional activation, subunit 9 (33kD)	0.472	0.157
Zinc finger protein 254	0.489	0.374
Ring finger protein 1	0.404	0.154
Nuclear respiratory factor 1	0.376	0.111
HSPC028 protein	0.486	0.009
KIAA0664 protein	0.496	0.031
signal transduction		
Regulator of G-protein signalling 4	0.109	0.029
Integrin, alpha 9	0.164	0.015
CAMP responsive element modulator	0.255	0.158
Endothelin receptor type B	0.302	0.011
AL514445 LTI_NFL006_PL2 Homo sapiens cDNA clone CL0BB010ZF08 3 prime, mRNA sequence.	0.322	0.008
Ankyrin 1, erythrocytic	0.340	0.094
wu94e06.x1 NCI_CGAP_Kid3 Homo sapiens cDNA clone IMAGE:2527714 3' similar to gb:U07358 MIXED LINEAGE KINASE 2 (HUMAN);, mRNA sequence.	0.342	0.098
ADP-ribosylation factor related protein 1	0.345	0.030
Melanoma cell adhesion molecule	0.351	0.053
7o43e03.x1 NCI_CGAP_Kid11 Homo sapiens cDNA clone IMAGE:3577036 3', mRNA sequence.	0.431	0.095
LIM domain only 7	0.439	0.045
Enigma (LIM domain protein)	0.492	0.036
RNA binding		
qb33c06.x1 Soares_pregnant_uterus_NbHPU Homo sapiens cDNA clone IMAGE:1698058 3', mRNA sequence.	0.215	0.055
RNA binding motif protein 12	0.386	0.007

Table II. Continued

gene	foldchange	t-test p-value
RNA binding		
Polyadenylate binding protein-interacting protein 1	0.411	0.029
Splicing factor, arginine/serine-rich 6	0.419	0.003
AU146237 HEMBA1 Homo sapiens cDNA clone HEMBA1007233 3', mRNA sequence.	0.422	0.013
Polyadenylate binding protein-interacting protein 1	0.458	0.058
Splicing factor, arginine/serine-rich 7 (35kD)	0.472	0.060
DEAD-box protein abstrakt	0.493	0.035
Mitochondrial ribosomal protein L12	0.495	0.138
Heterogeneous nuclear ribonucleoprotein D-like	0.497	0.025
transport		
wc46f12.x1 NCI_CGAP_Pr28 Homo sapiens cDNA clone IMAGE:2321711 3' similar to TR:O14564 O14564 HYPOTHETICAL 67.1 KD PROTEIN. ;, mRNA sequence.	0.338	0.072
Uncoupling protein 2 (mitochondrial, proton carrier)	0.385	0.020
Adaptor-related protein complex 3, sigma 2 subunit	0.278	0.110
Solute carrier family 4, anion exchanger, member 2 (erythrocyte membrane protein band 3-like 1)	0.408	0.134
Hypothetical protein FLJ14038	0.469	0.002
Solute carrier family 4, sodium bicarbonate cotransporter-like, member 10	0.395	0.124
N amino acid transporter 3	0.451	0.072
Solute carrier family 25 (mitochondrial carrier; oxoglutarate carrier), member 11	0.467	0.017
Solute carrier family 19 (folate transporter), member 1	0.490	0.068
cell proliferation		
Deoxyhypusine synthase	0.175	0.026
Deoxyhypusine synthase	0.372	0.039
ba69f11.x1 NIH_MGC_20 Homo sapiens cDNA clone IMAGE:2905677 3' similar to SW:CL6_RAT Q08755 INSULIN-INDUCED GROWTH RESPONSE PROTEIN CL-6 ;, mRNA sequence.	0.437	0.008
Cyclin H	0.455	0.043
Bridging integrator 1	0.487	0.071
V-Ki-ras2 Kirsten rat sarcoma 2 viral oncogene homolog	0.489	0.171
Deoxyhypusine synthase	0.494	0.031
U69567 Soares infant brain 1NIB Homo sapiens cDNA clone c-2mell, mRNA sequence.	0.499	0.072
DNA metabolism		
BRCA1-interacting protein 1; BRCA1-associated C-terminal helicase 1	0.410	0.028
Uracil-DNA glycosylase	0.434	0.102
Nth (E.coli endonuclease III)-like 1	0.443	0.017
DNA (cytosine-5-)-methyltransferase 2	0.469	0.209
602504673F1 NIH_MGC_77 Homo sapiens cDNA clone IMAGE:4617907 5', mRNA sequence.	0.470	0.200

are indispensable for protein synthesis (Christensen, 1990; McGivan and Pastor-Anglada, 1994). Among the amino acid transport systems described, system L is a major rout for providing cells with large neutral amino acids including branched or aromatic amino acids (Cornford *et al.*, 1992; Gomes and Soares-da-Silva, 1999). LAT1 is a system L amino acid transporter which transports a lot of essential amino acids. It is proposed to be at least one of the amino acids transporters essential for tumor cell growth (Yanagida *et al.*, 2001). High level of expression of LAT1 in tumor cells was indicated in tumor masses of various tissue origins as well as various tumor cell lines to support the high protein synthesis for cell growth and cell activation (Kanai *et al.*, 1998; Sang *et al.*, 1995; Wolf *et al.*, 1996). Since LAT1 is an amino acid transporter essential for tumor cell growth, one can expect that inhibition of LAT1 function may be a rational to anti-cancer therapy to suppress tumor growth (Kim *et al.*, 2004). BCH

is an amino acid-related compound which has been used as a selective inhibitor of system L (Christensen, 1990; Christensen *et al.*, 1969). Our previous studies have shown that BCH exert inhibitory effects on T24 cells through inhibition of LAT1 (Kim *et al.*, 2002). We confirmed this for T24 cells by showing that BCH in logarithmic phase of cell growth curve inhibits cell proliferation (Fig. 1).

Determining of gene expression profiles of T24 bladder carcinoma cells after BCH treatment is important for designing new anticancer drugs. It is possible to analyze the expression profiles of a large number of genes simultaneously using microarray. In this study, we utilized the high throughput gene chip, which contains 39,000 known genes, to determine the alternation of gene expression profiles of T24 bladder carcinoma cells exposed to BCH. Our results from cDNA microarray provided a complex cellular and molecular response to BCH treatment that likely to be mediated by a variety of regulatory pathways. We found that the molecular response to BCH in T24 bladder carcinoma cells involved inhibition or induction of genes that are related to biochemical, biological and regulatory processes in the cells. These genes have specific functions in cell proliferation, DNA metabolism, enzyme reaction, RNA binding, signal transduction, transcription, and transport. General tendency was up-regulation of these genes at 3 h and down-regulation at 12 h after BCH treatment (Fig. 2 and 3). These results suggest that inhibition of LAT1 by BCH may modulate the expression of first-response genes at an earlier stage (3 h), and in turn, alter the expression of intracellular second messenger molecules, resulting in cell adaptation for survival. At later stage (12 h), cellular response to BCH may involve modulation of gene expression for cell growth inhibition. For example up regulation of genes that are involved in cell proliferation at 3 h provide cellular pathways for survival and adaptation whereas down regulation of this group of genes at 12 h inhibit cell growth. Expression of interleukin 1 that stimulates proliferation (Beales, 2002; Kaden *et al.*, 2003; Olman *et al.*, 2002), significantly increased after 3 h and expression of deoxyhypusine synthase that causes growth in mammalian cells (Chen *et al.*, 1996; Park *et al.*, 1994; Shi *et al.*, 1996) decreased after 12 h, suggesting that BCH may inhibit cell growth through regulation of the expression of these important genes related to cell proliferation.

In signal transduction group, up regulation of Sorting nexin 11, GRO2 oncogene, Epiregulin, Adenosine A1 receptor, Inhibin alpha and down regulation of KIAA1075 protein were observed at 3 h whereas down regulation of Regulator of G-protein signalling 4, Integrin alpha 9, Endothelin receptor type B, ADP-ribosylation factor related protein 1, LIM domain only 7, Enigma (LIM domain protein) and up regulation of Hypothetical protein and Opsin 3 (encephalopsin, panopsin) were observed at 12 h, suggesting that cell signal transduction pathways is important for cell growth inhibition *via* LAT1 inhibitor.

In summary, we have analyzed the gene expression profiles of T24 bladder carcinoma cells exposed to BCH. BCH altered the expressions of many genes that are related to the control of cell proliferation, DNA metabolism, enzyme reaction, RNA binding, signal transduction, transcription, and transport. The gene expression profiles revealed novel molecular mechanisms by which BCH exerts its inhibitory effects on bladder carcinoma. BCH-induced regulation of these genes may be exploited for mechanism-based therapeutic strategies and new drugs development for bladder carcinoma. However, further in-depth studies are required to investigate the effects of BCH on the regulation of important cellular molecules at the protein levels to examine the effects of BCH on cellular pathways.

REFERENCES

Beales, I. L., Effect of Interlukin-1â on proliferation of gastric epithelial cells in culture. *BMC Gastroenterol.*, 2, 7 (2002).

Chen, Z. P., Yan, Y. P., Ding, Q. J., Knapp, S., Potenza, J. A., Schugar, H. J., and Chen, K. Y., Effects of inhibitors of deoxyhypusine synthase on the differentiation of mouse neuroblastoma and erythroleukemia cells. *Cancer lett.*, 105, 233-239 (1996).

Christensen, H. N., Role of amino acid transport and countertransport in nutrition and metabolism. *Physiol. Rev.*, 70, 43-77 (1990).

Christensen, H. N., Handlogten, M. E., Lam, I., Tager, H. S., and Zand, R., A bicyclic amino acid to improve discriminations among transport systems. *J. Biol. Chem.*, 244, 1510–1520 (1969).

Cornford, E. M., Young, D., Paxton, J. W., Finlay, G. J., Wilson, W. R., and Pardridge, W. M., Melphalan penetration of the blood-brain barrier via the neutral amino acid transporter in tumor-bearing brain. *Cancer Res.*, 52, 138-143 (1992).

Gomes, P. and Soares-da-Silva, P., L-DOPA transport properties in an immortalised cell line of rat capillary cerebral endothelial cells, RBE 4. *Brain Res.*, 829, 143-150 (1999).

Kaden, J. J., Dempfle, C. E., Grobholz, R., Tran, H. T., Kilic, R., Sarikoc, A., Brueckmann, M., Vahl, C., Hagl, S., Haase, K. K., and Borggrefe, M., Interleukin-1 beta promotes matrix metalloproteinase expression and cell proliferation in calcific aortic valve stenosis. *Atherosclerosis*, 170, 205-211 (2003).

Kanai, Y. and Endou, H., Heterodimeric amino acid transporters: molecular biology and pathological and pharmacological relevance. *Curr. Drug Metab.*, 2, 339-354 (2001).

Kanai, Y., Segawa, H., Miyamoto, K., Uchino, H., Takeda, E., and Endou, H., Expression cloning and characterization of a transporter for large neutral amino acids activated by the

heavy chain of 4F2 antigen (CD98). *J. Biol. Chem.*, 273, 23629–23632 (1998).

Kanno, J., Aisaki, K. I., Igarashi, K., Nakatsu, N., Ono, A., Kodama, Y., and Nagao, T., "Per cell" normalization method for mRNA measurement by quantitative PCR and microarrays. *BMC Genomics*, 7, 64 (2006).

Kim, D. K., Kanai, Y., Choi, H. W., Tangtrongsup, S., Chairoungdua, A., Babu, E., Tachampa, K., Anzai, N., Iribe, Y., and Endou, H., Characterization of the system L amino acid transporter in T24 human bladder carcinoma cells. *Biochim. Biophys. Acta*, 1565, 112-121 (2002).

Kim, D. K., Kim, I. J., Hwang, S., Kook, J. H., Lee, M. C., Shin, B. A., Bae, C. S., Yoon, J. H., Ahn, S. G., Kim, S. A., Kanai, Y., Endou, H., and Kim, J. K., System L-amino acid transporters are differently expressed in rat astrocyte and C6 glioma cells. *Neurosci. Res.*, 50, 437-446 (2004).

Li, Y. and Sarkar, F. H., Gene expression profiles of genistein-treated PC3 prostate cancer cells. *J. Nutr.*, 132, 3623-3631 (2002).

Macgregor, P. F. and Squire, J. A., Application of microarrays to the analysis of gene expression in cancer. *Clin. Chem.*, 48, 1170-1177 (2002).

McGivan, J. D. and Pastor-Anglada, M., Regulatory and molecular aspects of mammalian amino acid transport. *Biochem. J.*, 299, 321-334 (1994).

Olman, M. A., White, K. E., Ware, L. B., Cross, M. T., Zhu, S., and Matthay, M. A., Microarray analysis indicates that pulmonary edema fluid from patients with acute lung injury mediates inflammation, mitogen gene expression, and fibroblast proliferation through bioactive interleukin-1. *Chest*, 121 Suppl 3, 69-70 (2002).

Oxender, D. L. and Christensen, H. N., Evidence for two types of mediation of neutral amino acid transport in Ehrlich cells. *Nature*, 197, 765-767 (1963).

Park, M. H., Wolff, E. C., Lee, Y. B., and Folk, J. E., Antiproliferative effects of inhibitors of deoxyhypusine synthase. Inhibition of growth of Chinese hamster ovary cells by guanyl diamines. *J. Biol. Chem.*, 269, 27827-27832 (1994).

Sang, J., Lim, Y. P., Panzia, M., Finch, P., and Thompson, N. L., TA1, a highly conserved oncofetal complementary DNA from rat hepatoma, encodes an integral membrane protein associated with liver development, carcinogenesis, and cell activation. *Cancer Res.*, 55, 1152-1159 (1995).

Shi, X. P., Yin, K. C., Ahern, J., Davis, L. J., Stern, A. M., and Waxman, L., Effects of N1-guanyl-1, 7-diaminoheptane, an inhibitor of deoxyhypusine synthase, on the growth of tumorigenic cell lines in culture. *Biochim. Biophys. Acta*, 1310, 119-126 (1996).

Wolf, D. A., Wang, S., Panzia, M. A., Bassily, N. H., and Thompson, N. L., Expression of a highly conserved oncofetal gene, TA1/E16, in human colon carcinoma and other primary cancers: homology to Schistosoma mansoni amino acid permease and Caenorhabditis elegans gene products. *Cancer Res.*, 56, 5012-5022 (1996).

Yanagida, O., Kanai, Y., Chairoungdua, A., Kim, D. K., Segawa, H., Nii, T., Cha, S. H., Matsuo, H., Fukushima, J., Fukasawa, Y., Tani, Y., Taketani, Y., Uchino, H., Kim, J. Y., Inatomi, J., Okayasu, I., Miyamoto, K., Takeda, E., Goya, T., and Endou, H., Human L-type amino acid transporter 1 (LAT1): characterization of function and expression in tumor cell lines. *Biochim. Biophys. Acta*, 1514, 291-302 (2001).

0026-895X/07/7205-1171–1180$20.00
MOLECULAR PHARMACOLOGY
Copyright © 2007 The American Society for Pharmacology and Experimental Therapeutics
Mol Pharmacol 72:1171–1180, 2007

Vol. 72, No. 5
38836/3268509
Printed in U.S.A.

Evaluation of Action Mechanisms of Toxic Chemicals Using JFCR39, a Panel of Human Cancer Cell Lines[S]

Noriyuki Nakatsu, Tomoki Nakamura, Kanami Yamazaki, Soutaro Sadahiro, Hiroyasu Makuuchi, Jun Kanno, and Takao Yamori

Division of Molecular Pharmacology, Cancer Chemotherapy Center, Japanese Foundation for Cancer Research, Koto-ku, Tokyo, Japan (N.N., T.N., K.Y., T.Y.); Division of Cellular and Molecular Toxicology, Biological Safety Research Center, National Institute of Health Sciences, Setagaya-ku, Tokyo, Japan (N.N., J.K.); and Second Department of Surgery, Tokai University School of Medicine, Boseidai, Isehara-City, Kanagawa, Japan (T.N., S.S., H.M.)

Received June 6, 2007; accepted August 16, 2007

ABSTRACT

We previously established a panel of human cancer cell lines, JFCR39, coupled to an anticancer drug activity database; this panel is comparable with the NCI60 panel developed by the National Cancer Institute. The JFCR39 system can be used to predict the molecular targets or evaluate the action mechanisms of the test compounds by comparing their cell growth inhibition profiles (i.e., fingerprints) with those of the standard anticancer drugs using the COMPARE program. In this study, we used this drug activity database-coupled JFCR39 system to evaluate the action mechanisms of various chemical compounds, including toxic chemicals, agricultural chemicals, drugs, and synthetic intermediates. Fingerprints of 130 chemicals were determined and stored in the database. Sixty-nine of 130 chemicals (~60%) satisfied our criteria for the further analysis and were classified by cluster analysis of the fingerprints of these chemicals and several standard anticancer drugs into the following three clusters: 1) anticancer drugs, 2) chemicals that shared similar action mechanisms (for example, ouabain and digoxin), and 3) chemicals whose action mechanisms were unknown. These results suggested that chemicals belonging to a cluster (i.e., a cluster of toxic chemicals, a cluster of anticancer drugs, etc.) shared similar action mechanism. In summary, the JFCR39 system can classify chemicals based on their fingerprints, even when their action mechanisms are unknown, and it is highly probable that the chemicals within a cluster share common action mechanisms.

Determining the action mechanism or identifying the molecular target of a chemical with pharmacological activity or adverse side effects is highly desirable. Although various test methods are currently available for determining the action mechanisms of chemicals, such as methods based on animal models, methods based on cellular models, bacterial mutagenicity test, the uterotropic assay (Kanno et al., 2002), Hershberger test (Hershberger et al., 1953), and the reporter assay for the nuclear receptor agonists, determination of the action mechanisms of pharmacologically active chemicals, including the toxic chemicals, is still a difficult and challenging task. Therefore, it is highly desirable to develop efficient test methods for evaluating toxicity of chemicals.

A number of screening methods are currently available for discovering new anticancer drugs. One very powerful and unique approach using multiple cancer cell lines was developed at NCI (Paull et al., 1989; Weinstein et al., 1992, 1997) and in our laboratory (Yamori et al., 1999; Dan et al., 2002, 2003; Yamori, 2003; Nakatsu et al., 2005; Akashi and Yamori, 2007; Akashi et al., 2007; Nakamura et al., 2007). This bioinformatics-based approach enables mechanism-oriented evaluation of anticancer drugs. For example, we can evaluate the cell toxicity in vitro by determining the 50% growth inhibition (GI50), total growth inhibition, and 50% lethal concentration across a panel of 39 human cancer cell lines (JFCR39). We can also predict the molecular targets or evaluate the action mechanisms of the test compounds by comparing the cell growth inhibition profiles (termed "fingerprints") across the panel for these compounds with those of

This work was supported in part by Grant-in-Aid 17390032 for Scientific Research (B) from Japan Society for the Promotion of Science (to T.Y.); Ministry of Health, Labor, and Welfare Grants-in-Aid H15-kagaku-002, H16-kagaku-003 (to T.Y. and J.K.); Grant-in-Aid 18015049 of the Priority Area "Cancer" from the Ministry of Education, Culture, Sports, Science and Technology of Japan (to T.Y.); and grant 05-13 from National Institute of Biomedical Innovation Japan (to T.Y.)

N. N. and T. N. equally contributed to this study.

Article, publication date, and citation information can be found at http://molpharm.aspetjournals.org.

doi:10.1124/mol.107.038836.

[S] The online version of this article (available at http://molpharm.aspetjournals.org) contains supplemental material.

ABBREVIATIONS: GI50, 50% growth inhibition concentration; GI50, 50% growth inhibition; SN-38, 7-ethyl-10-hydroxycamptothecin; SV-NN, snake venom from *N. nigricollis*; SV-NNK; snake venom from *N. naja kaouthia*.

TABLE 1
List of chemicals tested. Chemical names, abbreviations, and applications/targets/mechanisms of the test compounds are summarized.

JCI No	Name	Abbreviation	Application/Target/Mechanism
−691	Trioctyltin	TOT	Organotin
−690	Triphenyltin	TPT	Organotin
−689	Dibutyltin		Organotin
−688	AM-580		RARα
−687	TTNPB		RAR
−686	13-*cis* Retinoic acid	13-*cis*	RAR
−607	Methoprene		Agricultural chemical
−606	Methoprene acid		RXR
−605	5-aza-2′-deoxycytidine	5-AzaC	Methylation
−604	Carbaryl		Agricultural chemical
−603	Acephate		Agricultural chemical
−602	Sodium arsenite		Agricultural chemical
−601	Testosterone propionate	TP	Testosterone
−600	Ethynyl estradiol	EE	Estrogenic
−599	Thiram		Agricultural chemical
−598	Dimethylformamide	DMF	Solvent
−568	α-Bungarotoxin	αBuTX	Neurotoxin
−567	Snake venom from *Trimeresurus flavoviridis*	SV-TF	Snake venom
−566	Snake venom from *Crotalus atrox*	SV-CA	Snake venom
−565	Snake venom from *Agkistrodon halys blomhoffii*	SV-AHB	Snake venom
−564	Dexamethasone	DEX	Steroid
−563	3-Methylcholanthrene	3-MC	Teratogenicity/carcinogenicity
−562	*N*-Ethyl-*N*-nitrosourea	ENU	Teratogenicity/carcinogenicity
−561	Diethylnitrosamine	DEN	Teratogenicity/carcinogenicity
−560	All *trans*-retinoic acid	ATRA	RAR + RXR
−559	9-cis Retinoic acid	9-cis	RAR
−558	Levothyroxine	T4	Thyroid hormone
−557	3-Amino-1*H*-1,2,4-triazole	3AST	Agricultural chemical
−555	2-Vinylpyridine	2VP	Synthetic intermediate
−553	Phenobarbital	PB	Antiepileptic
−552	Acetaminophen	APAP	Analgetic
−551	Isoniazid		Phthisic
−549	4-Ethylnitrobenzene	4ENB	Synthetic intermediate
−548	1,2-Dichloro-3-nitrobenzene	1,2DC3NB	Pigment/synthetic intermediate
−546	*N*-Methylaniline	NMA	Synthetic intermediate
−545	2-Aminomethylpyridine	2AMP	Synthetic intermediate
−544	1*H*-1,2,4-Triazole		Synthetic intermediate
−543	1*H*-1,2,3-Triazole		Synthetic intermediate
−542	4-Amino-2,6-dichlorophenol	4A2,6DCP	Synthetic intermediate
−541	2,4-Dinitrophenol	2,4 DNP	Agricultural chemical
−513	Capsaicin		Food constituent
−485	2-Methoxyestradiol		Estrogenic
−466	Colcemid		Spindle inhibitor
−465	2,4-Dinitrochlorobenzene	2,4DCB	Pigment/mutagenesis
−464	Troglitazone		Diabetic
−463	Clofibrate		Antilipemic
−459	Bis(2-ethylhexyl)phthalate	DEHP	Plasticizer
−458	Thiourea		Agricultural chemical
−447	Cacodylic acid		Agricultural chemical
−446	Amitrole		Agricultural chemical
−445	4-Octylphenol	OP	Reproductive effector
−444	2,6-Dimethylaniline	2,6-Xylidene	Natural product
−443	1,2-Dibromo-3-chloropropane	DBCP	Agricultural chemical
−442	1,1-Dimethylhydrazine	1,1DMH	Reproductive effector
−441	Sulfanylamide		Agricultural chemical
−440	Streptozotocin		Agricultural chemical
−439	Spironolactone		Aldosterone antagonist
−438	*para*-Aminoazobenzene	pAAB	Pigment/mutagenicity/carcinogenicity
−437	*para*-Cresidine		Pigment/carcinogenicity
−436	Neostigmine bromide		Parasympathomimetics
−435	*para*-Dichlorobenzene	pDCB	Pigment/Agricultural chemical
−434	Phenytoin		Antiepileptic
−433	*ortho*-Toluidine	oToluidine	Pigment
−432	Imipramine		Antidepressant
−431	Cobalt chloride		Teratogenicity/mutagenicity
−428	Atrazine		Agricultural chemical
−427	Propylthiouracil		Teratogenicity/carcinogenicity
−426	Thalidomide (L + D)		Teratogenicity
−425	Carbon tetrachloride	CCl_4	Teratogenicity/carcinogenicity
−424	Hydroquinone		Oxidative stress
−423	Monocrotaline		Mutagenicity/carcinogenicity
−422	Vinyl chloride		Carcinogenicity
−421	Tributyltin chloride	TBT	Ship bottom paint/organotin
−420	Valproic acid		Antiepileptic
−419	Benzene		Carcinogenicity

TABLE 1—(*Continued*)

JCI No	Name	Abbreviation	Application/Target/Mechanism
−418	Acrylamide		Neurotoxin/carcinogenicity
−417	Hexachlorobenzene	BHC	Agricultural chemical/carcinogenicity
−346	2-Deoxyglucose	2-DG	Glycolytic pathway/glycosylation inhibitor
−325	Pentachlorophenol	PCP	Agricultural chemical/teratogenicity/carcinogenicity
−324	Aniline		Oxidative stress/methemoglobinemia/carcinogenicity
−323	Triazine		Agricultural chemical
−322	Edifenphos	EDDP	Agricultural chemical/antibiotics/choline esterase
−321	γ-1,2,3,4,5,6-Hexachlorocyclohexane	γ-BHC	Agricultural chemical/carcinogenicity
−320	Dichlorvos	DDVP	Agricultural chemical/teratogenicity/carcinogenicity
−319	*O*-Ethyl *O*-4-nitrophenyl phenylphosphonothioate	EPN	Agricultural chemical
−318	Cadmium chloride	$CdCl_2$	Teratogenicity/carcinogenicity
−317	Phenylmercury acetate	PMA	Fungicides/mutagenicity
−316	Mercaptoacetic acid		Synthetic intermediate
−315	1,3-Diphenylguanidine	DPG	Vulcanizing agent
−314	3,4,4'-Trichlorocarbanilide	TCC	Cosmetics/antibacterial agent
−313	3-Iodo-2-propynyl butylcarbamate	IPBC	Antibacterial agent
−311	2,3,3,3−2',3',3',3'-Octachlorodipropylether	S-421	Agricultural chemical/antibacterial agent
−310	1,2-Benzisothiazolin-3-one	BIT	Antibacterial agent
−309	Isobornylthiocyanoacetate	IBTA	Antibacterial agent
−308	*p*-Chlorophenyl-3-iodopropargylformal	CPIP	Antibacterial agent
−307	Zinc butylxanthate	ZBX	Vulcanizing agent
−306	Polypropylene glycol	PG	Synthetic intermediate
−305	10,10'-Oxy-bis(phenoxyarsine)	OBPA	Antibacterial agent
−296	Snake venom from *Naja naja kaouthia*	SV-NNK	Snake venom
−295	Snake venom from *Naja nigricollis*	SV-NN	Snake venom
−294	2,5-di(*tert*-butyl)-1,4-Hydroquinone	DTBHQ	Oxidative stress
−293	Ibotenic Acid		Mushroom toxin/neurotoxin
−292	*N*-Methy-4-phenyl-1,2,3,6-tetrahydropyridine	MPTP	Neurotoxin
−289	Tetrodotoxin		Natural product/Na^+ channel inhibitor
−288	ICI 182,780		Estrogen antagonist
−275	Benzophenone		Agricultural chemical
−274	1,2-Dibromo-3-chloropropane	DBCP	Antibacterial agent/insecticide/carcinogenicity
−273	Zineb		Agricultural chemical
−272	Dieldrin		Insecticide
−271	Hexachlorobenzene	HCB	Antibacterial agent/carcinogenicity
−270	Ziram		Antibacterial agent/vulcanizing agent
−269	Chlordane		Insecticide/carcinogenicity
−268	4,4'-Dichlorodiphenyltrichloroethane	p,p'-DDT	Insecticide/carcinogenicity/teratogenicity
−267	Bisphenol A	BPA	Estrogenic
−266	17-β-Estradiol	E2	Estrogenic
−265	Diethylstilbestrol	DES	Estrogenic
−261	Paraquat		Agricultural chemical/oxidative stress
−247	Ouabain		Cardiac glycosides
−245	Okadaic acid		Natural product/PP1, PP2A inhibitor
−242	Antimycin A1		Agricultural chemical
−232	Digoxin		Cardiac glycosides
−201	OH-Flutamide		Flutamide derivative/androgen antagonist
−200	Flutamide		Anticancer drugs/androgen antagonist
−185	30% H_2O_2		Oxidative stress
−182	*N*-Acetyl-L-cysteine	NAC	Super oxyside scavenger
−181	L-Ascorbic acid		Food constituent
−179	Dopamine		Neurotransmitter
−177	Caffeine		Food constituent
−168	Cycloheximide		Protein synthesis inhibitor
−144	4-Hydroxyphenylretinamide	4-HPR	RAR
−137	Indomethacin		COX inhibitor
−99	SN-38		Irinotecan derivative/Topo I
−96	Toremifene		Anticancer drugs/estrogen antagonist
−95	Tamoxifen		Anticancer drugs/estrogen antagonist
−63	Cyclosporin A		Anticancer drugs/helper T cell
−46	HCFU		Anticancer drugs/antimetabolite(pyrimidine)
−36	Docetaxel		Anticancer drugs/tubulin
−35	Paclitaxel		Anticancer drugs/tubulin
−34	Colchicine		Antipodagric/tubulin
−33	Cisplatin		Anticancer drugs/DNA cross linker
−32	Carboplatin		Anticancer drugs/DNA cross linker
−31	Irinotecan		Anticancer drugs/Topo I
−30	Camptothecin	CPT	Anticancer drugs/Topo I
−24	Methotrexate		Anticancer drugs/DHFR
−19	Vincristine		Anticancer drugs/tubulin
−18	Vinblastine		Anticancer drugs/tubulin
−16	Mitomycin-C	MMC	Anticancer drugs/DNA alkylator
−9	Tegafur		Anticancer drugs/antimetabolite(pyrimidine)
−8	5-Fluorouracil	5-FU	Anticancer drugs/antimetabolite(pyrimidine)
−5	Cytarabine		Anticancer drugs/antimetabolite(pyrimidine)
−4	Nitrogen mustard		Anticancer drugs/DNA alkylator

RAR, retinoic acid receptor; RXR; retinoid X receptor.

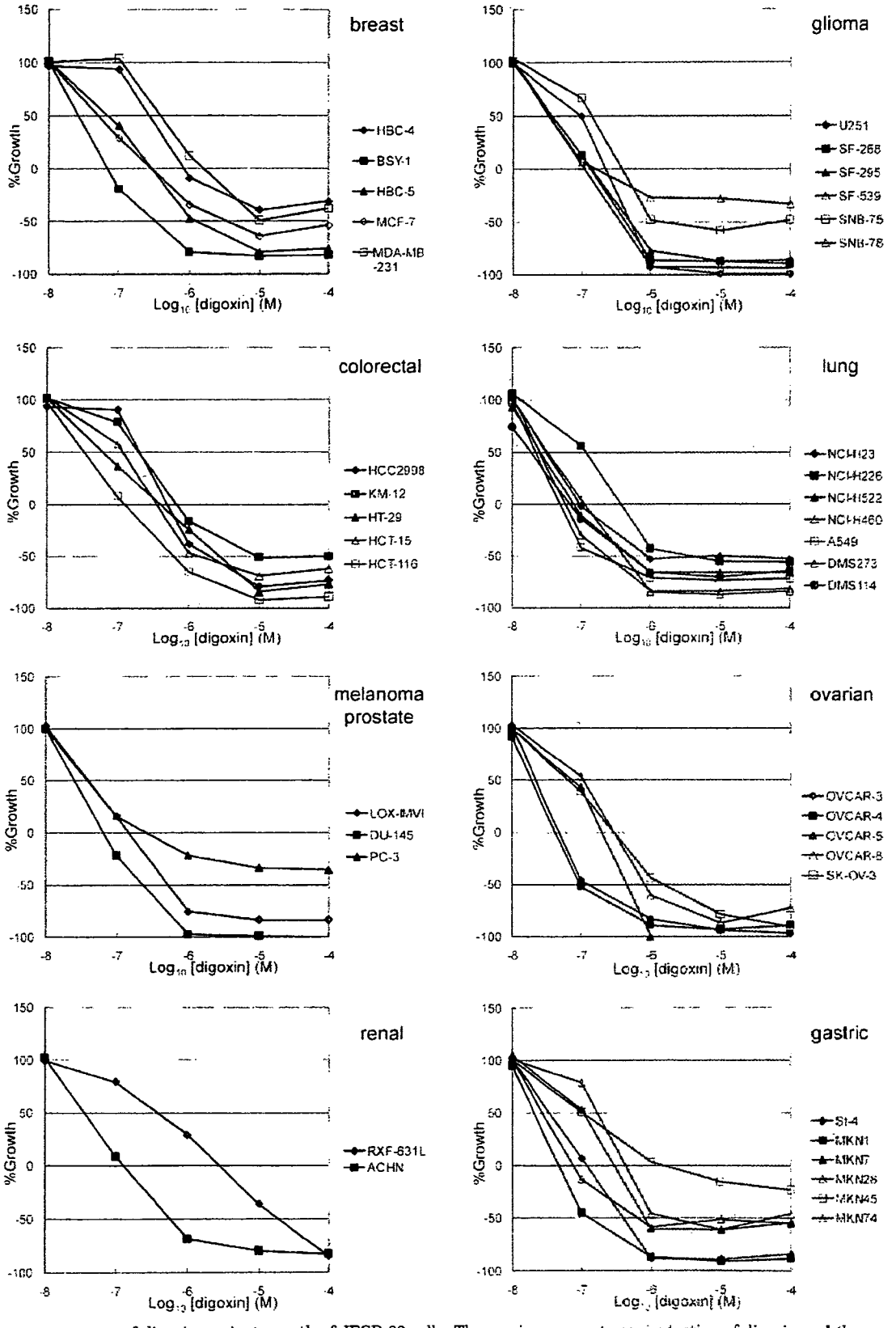

Fig. 1. Dose response curves of digoxin against growth of JFCR-39 cells. The *x*-axis represents concentration of digoxin and the *y-axis* represents percentage growth. The GI50 represents the concentration required to inhibit cell growth by 50% compared with untreated controls.

the standard anticancer drugs using the COMPARE algorithm (Yamori et al., 1999). We have used this system successfully and demonstrated that the molecular targets of the novel chemicals MS-274, FJ5002, and ZSTK474 were topoisomerases I and II (Yamori et al., 1999), telomerase (Naasani et al., 1999), and phosphatidylinositol 3-kinase (Yaguchi et al., 2006), respectively. Several other interesting studies, based on a panel of cancer cells, classified anticancer drugs according to their action mechanisms or molecular targets by cluster analysis of their GI50 values (Weinstein et al., 1992, 1997; Dan et al., 2002). Correlation analysis has also been used to explore the genes associated with the sensitivity of the cells in the panel to anticancer drugs (Scherf et al., 2000; Okutsu et al., 2002; Zembutsu et al., 2002; Nakatsu et al., 2005).

In this study, we have examined the potential of the JFCR39 system in classifying various chemicals, and predicted their action mechanisms. For this purpose, we have determined the fingerprints of 130 different types of chemicals including toxic chemicals, pesticides, drugs and synthetic intermediates, and then classified these chemicals according to the cluster analysis of their fingerprints.

Materials and Methods

Cell Lines and Cell Cultures. The panel of human cancer cell lines has been described previously (Yamori et al., 1999; Dan et al., 2002) and consists of the following 39 human cancer cell lines: lung cancer, NCI-H23, NCI-H226, NCI-H522, NCI-H460, A549, DMS273, and DMS114; colorectal cancer, HCC-2998, KM-12, HT-29, HCT-15, and HCT-116; gastric cancer, MKN-1, MKN-7, MKN-28, MKN-45, MKN-74, and St-4; ovarian cancer, OVCAR-3, OVCAR-4, OVCAR-5, OVCAR-8, and SK-OV-3; breast cancer, BSY-1, HBC-4, HBC-5, MDA-MB-231, and MCF-7; renal cancer, RXF-631L and ACHN; melanoma, LOX-IMVI; glioma, U251, SF-295, SF-539, SF-268, SNB-75, and SNB-78; and prostate cancer, DU-145 and PC-3. All cell lines were cultured in RPMI 1640 medium (Nissui Pharmaceutical, Tokyo, Japan) with 5% fetal bovine serum, penicillin (100 units/ml), and streptomycin (100 μg/ml) at 37°C under 5% CO_2.

Determination of Cell Growth Inhibition Profiles. Growth inhibition experiments were performed to assess the sensitivity of the cells to various chemicals as described before (Yamori et al., 1999; Dan et al., 2002). Growth inhibition was measured by determining the changes in the amounts of total cellular protein after 48 h of chemical treatment using a sulforhodamine B assay. For each chemical, the growth assay was performed using a total of five different concentrations of the chemical (for example, 10^{-4}, 10^{-5},

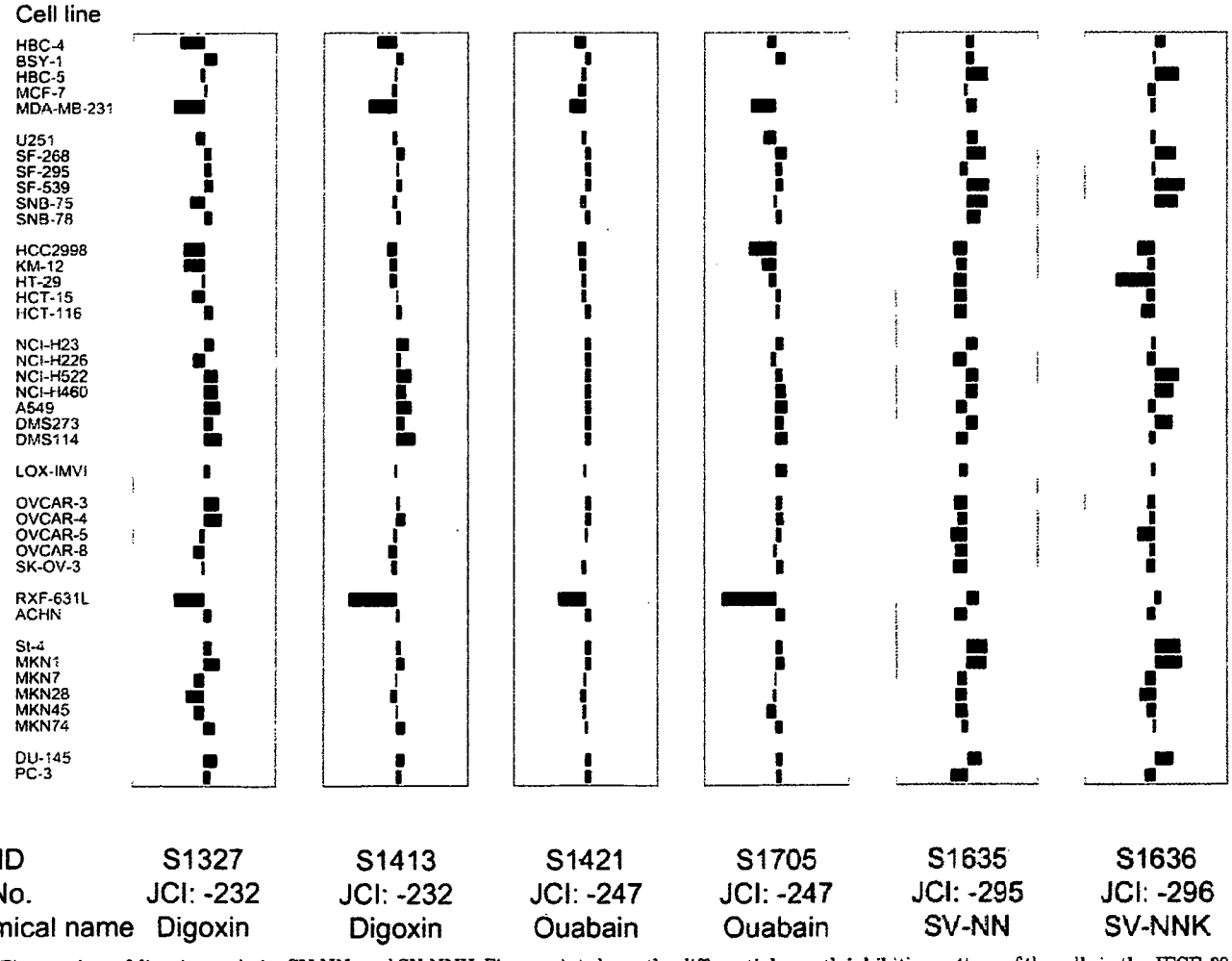

Fig. 2. Fingerprints of digoxin, ouabain, SV-NN, and SV-NNK. Fingerprint shows the differential growth inhibition pattern of the cells in the JFCR-39 panel against the test chemical. The *X*-axis represents relative value of GI50; $(-1) \times$ (log GI50 − MG-MID); MG-MID is the mean value of the log GI50. Zero means the mean GI50 and one means the GI50 value is 10-fold more sensitive than the mean GI50. Exp-ID and JCI numbers are the ID for the experiment and ID for the chemical, respectively, in our database.

10^{-6}, 10^{-7}, and 10^{-8} M) and one negative control. All assays were performed in duplicate. This GI50 calculation method is well established and reliable through anticancer drug screen using NCI60 as well as JFCR39 (Paull et al., 1989; Yamori et al., 1999; Yamori, 2003). At each test concentration, the percentage growth was calculated using the following seven absorbance measurements: growth at time 0 (T0), growth of the control cells (C), and test growth in the presence of five different concentrations (T) of a drug. The percentage growth inhibition was calculated as: % growth = $100 \times [(T - T0)/(C - T0)]$ when $T \geq T0$, and % growth = $100 \times [(T - T0)/T]$ when $T < T0$. The GI50 values, which represent 50% growth inhibition concentration, were calculated as $100 \times [(T - T0)/(C - T0)] = 50$. When the GI50 of a chemical could not be calculated, the highest used concentration was assigned as its GI50 value. Absolute values of GI50 were then log transformed for further analysis. We certified the accuracy of measured GI50 data by using reference control chemicals, such as mitomycin-C, paclitaxel, and SN-38, in every experiment and by checking the dose response curves.

Chemicals. Spironolactone, *para*-aminoazobenzene, *para*-cresidine, neostigmine bromide, *para*-dichlorobenzene, phenytoin, *ortho*-toluidine, imipramine, cobalt chloride, atrazine, propylthiouracil, (D,L)-thalidomide, carbon tetrachloride, hydroquinone, monocrotaline, vinyl chloride, tributyl-tin chloride, valproic acid, benzene, acrylamide, pentachlorophenol, aniline, 1,3-diphenylguanidine, polypropylene glycol, 10,10'-oxy-bis(phenoxyarsine), testosterone propionate, carbaryl, acephate, bisphenol A, 17-β-estradiol, diethylstilbestrol, and α-bungarotoxin were purchased from Wako (Tokyo, Japan). Snake venoms from *Agkistrodon halys blomhoffii*, *Trimeresurus flavoviridis*, *Crotalus atrox*, *Naja nigricollis*, and *Naja naja kaouthia* were purchased from Latoxan (Valence, France). 2-Aminomethylpyridine, 1*H*-1,2,4-triazole, 1*H*-1,2,3-triazole, 3,4,4'-trichlorocarbanilide, edifenphos, dichlorvos, *O*-ethyl *O*-4-nitrophenyl phenylphosphonothioate, 2,4-dinitrophenol, *N*-methylaniline, 1,2-dichloro-3-nitrobenzene, 4-ethylnitrobenzene, 2-vinylpyridine, 3-amino-1*H*-1,2,4-triazole, *N*-ethyl-*N*-nitrosourea, 5-aza-2'-deoxycytidine, ethynyl estradiol, 3-methylcholanthrene, phenobarbital, acetaminophen, isoniazid, capsaicin, *N*-deacetyl-*N*-methylcolchicine (Colcemid), 2,4-dinitrochlorobenzene, and dexamethasone were from Sigma Chemicals (St. Louis, MO). Methoprene acid, methoprene, all-*trans* retinoic acid, and 9-cis retinoic acid were from BIOMOL International L.P. (Plymouth Meeting, PA). Levothyroxine was from MP Biomedicals (Irvine, CA). 3-Iodo-2-propynyl butylcarbamate was from Olin Japan Inc. (Tokyo, Japan), *p*-chlorophenyl-3-iodopropargylformal was from Nagase ChemteX (Osaka, Japan), and 2,3,3,3–2',3',3',3'-octachlorodipropylether was from Sankyo Chemical Industries, Ltd. (Tokyo, Japan). 1,2-Benzisothiazolin-3-one was from Riverson (Osaka, Japan), zinc butylxanthate was from Ouchishinko Chemical Industrial Co., Ltd. (Tokyo, Japan), and 4-amino-2,6-dichlorophenol was from Tokyo Kasei Kogyo Co. Ltd. (Tokyo, Japan).

Hierarchical Clustering. Hierarchical clustering analysis was carried out using the average linkage method and the "GeneSpring" software (Silicon Genetics, Inc., Redwood, CA). Pearson correlation coefficients were used to determine the degree of similarity.

Results

Sensitivity of JFCR39 to Chemicals. Sensitivity of the JFCR39 panel of cells to 130 chemicals was determined as described under *Materials and Methods*. Table 1 summarizes

TABLE 2

Log_{10} GI50 values of chemicals for each cell line in the JFCR-39 panel

Hi-conc means the highest concentration of the test chemical used. When the growth inhibition was over 50% at the Hi-Conc, GI_{50} was assigned the Hi-Conc value.

Exp-ID	S3416	S3415	S3413	S3245	S3117	S3414	S3118	S3246	S3125	S3124	S3123	S1636	S1635	S1634	S1718
JCI No	−687	−686	−559	−559	−559	−560	−560	−560	−567	−566	−565	−296	−295	−294	−294
Name or Abbr.	TTNPB	13-*cis*	9-*cis*			ATRA			SV-TF	SV-CA	SV-AHB	SV-NNK	SV-NN	DTBHQ	
Hi-Conc.	−4	−4	−4	−4	−4	−4	−4	−4	−4	−4	−4	−4	−4	−4	−4
HBC-4	−4.76	−4.00	−4.53	−4.40	−4.43	−4.42	−4.41	−4.41	−5.87	−5.80	−5.66	−7.25	−7.31	−4.72	−4.80
BSY-1	−4.78	−4.16	−4.60	−4.73	−4.73	−4.69	−4.70	−4.81	−6.31	−6.06	−5.76	−6.93	−7.34	−5.07	−4.93
HBC-5	−4.80	−4.41	−4.56	−4.57	−4.61	−4.61	−4.47	−4.51	−6.98	−6.45	−5.73	−7.64	−7.72	−4.89	−4.78
MCF-7	−4.73	−4.35	−4.40	−4.39	−4.48	−4.48	−4.54	−4.66	−5.87	−5.78	−5.68	−6.77	−7.08	−5.29	−5.25
MDA-MB-231	−4.75	−4.21	−4.70	−4.55	−4.69	−4.63	−4.53	−4.65	−5.90	−5.86	−5.84	−6.84	−7.39	−5.52	−5.30
U251	−4.77	−4.14	−4.61	−4.51	−4.61	−4.57	−4.45	−4.63	−6.45	−5.76	−5.70	−6.85	−7.44	−4.96	−5.11
SF-268	−4.75	−4.00	−4.24	−4.55	−4.40	−4.47	−4.48	−4.76	−5.90	−5.79	−5.70	−7.53	−7.67	−4.77	−4.81
SF-295	−4.80	−4.29	−4.54	−4.66	−4.60	−4.59	−4.48	−4.57	−6.19	−5.80	−5.74	−6.89	−6.97	−4.87	−4.97
SF-539	−4.95	−4.35	−4.75	−4.80	−4.79	−4.80	−4.71	−4.76	−6.39	−5.96	−5.81	−7.79	−7.75	−4.79	−4.86
SNB-75	−5.31	−5.28	−5.13	−5.19		−4.71	−4.69	−4.87	−6.41	−6.33	−5.93	−7.60	−7.70	−4.67	−4.80
SNB-78	−4.77	−4.25	−4.69	−4.78	−4.86	−4.49	−4.70	−4.68	−6.19	−6.00	−5.95	−6.97	−7.53	−4.75	−4.75
HCC2998	−4.68	−4.00	−4.48	−4.61	−4.62	−4.55	−4.62	−4.76	−5.91	−5.75	−5.67	−6.47	−6.77	−4.82	−4.75
KM-12	−4.70	−4.00	−4.46	−4.51	−4.48	−4.51	−4.47	−4.58	−5.93	−5.80	−5.65	−6.77	−6.87	−4.74	−4.77
HT-29	−4.73	−4.00	−4.47	−4.53	−4.50	−4.60	−4.52	−4.56	−5.90	−5.80	−5.56	−5.89	−6.78	−4.80	−4.89
HCT-15	−4.72	−4.25	−4.45	−4.49	−4.48	−4.52	−4.57	−4.53	−5.88	−5.76	−5.57	−6.73	−6.82	−4.72	−4.77
HCT-116	−4.77	−4.07	−4.67	−4.59	−4.67	−4.71	−4.61	−4.64	−6.46	−6.10	−5.77	−6.58	−6.82	−4.98	−5.13
NCI-H23	−4.74	−4.00	−4.47	−4.60	−4.59	−4.61	−4.55	−4.63	−6.11	−5.75	−5.72	−6.86	−7.42	−4.76	−4.90
NCI-H226	−4.72	−4.00	−4.61	−4.68	−4.78	−4.80	−4.54	−5.48	−5.95	−5.81	−5.76	−6.73	−6.78	−4.89	−4.91
NCI-H522	−4.72	−4.45	−4.68	−4.82	−4.77	−4.71	−4.71	−4.68	−6.45	−5.99	−5.78	−7.62	−7.46	−5.37	−5.37
NCI-H460	−4.70	−4.00	−4.55	−4.63	−4.58	−4.68	−4.55	−4.49	−5.96	−5.82	−5.72	−7.44	−7.42	−4.84	−4.84
A549	−4.79	−4.00	−4.72	−4.77	−4.78	−4.70	−4.62	−4.53	−5.91	−5.79	−5.71	−6.80	−6.83	−4.83	−4.87
DMS273	−4.57	−4.21	−4.50	−4.62	−4.55	−4.57	−4.51	−4.49	−6.20	−5.81	−5.72	−7.43	−7.44	−4.91	−4.98
DMS114	−4.77	−4.16	−4.33	−4.62	−4.49	−4.51	−4.53	−4.61	−6.66	−6.33	−5.77	−6.83	−6.88	−5.12	−5.21
LOX-IMVI	−4.77	−4.69	−4.68	−4.66	−4.70	−4.77	−4.74	−4.74	−6.75	−6.59	−5.76	−6.86	−6.94	−5.05	−5.15
OVCAR-3	−4.77	−4.38	−4.56	−4.67	−4.72	−4.64	−4.62	−4.71	−6.61	−6.13	−5.89	−6.77	−6.79	−4.89	−4.86
OVCAR-4	−4.72	−4.05	−4.63	−4.64	−4.64	−4.58	−4.39	−4.54	−6.73	−6.23	−5.80	−6.82	−6.90	−5.13	−4.90
OVCAR-5	−4.75	−4.00	−4.33	−4.39	−4.42	−4.44	−4.34	−4.44	−5.92	−5.74	−5.67	−6.46	−6.71	−5.22	−5.26
OVCAR-8	−4.75	−4.23	−4.50	−4.53	−4.59	−4.66	−4.67	−4.70	−5.95	−5.77	−5.69	−6.82	−6.84	−4.64	−4.70
SK-OV-3	−4.79	−4.00	−4.49	−4.51	−4.81	−4.52	−4.54	−4.50	−5.76	−5.64	−4.91	−6.75	−6.76	−4.64	−4.74
RXF-631L	−4.77	−4.00	−4.54	−4.58	−4.60	−4.72	−4.63	−4.61	−5.91	−5.80	−5.59	−7.13	−7.46	−4.81	−4.84
ACHN	−4.73	−4.00	−4.56	−4.66	−4.56	−4.50	−4.40	−4.76	−5.90	−5.79	−5.73	−6.74	−6.80	−4.71	−4.83
St-4	−4.74	−4.00	−4.42	−4.54	−4.65	−4.53	−4.49	−4.57	−5.91	−5.81	−5.76	−7.65	−7.70	−4.68	−4.75
MKN1	−4.75	−4.33	−4.56	−4.63	−4.62	−4.56	−4.45	−4.48	−6.15	−5.81	−5.78	−7.67	−7.68	−4.59	−4.81
MKN7	−4.78	−4.40	−4.68	−4.59	−4.70	−4.73	−4.56	−4.65	−6.29	−5.85	−5.76	−6.70	−6.90	−4.79	−4.84
MKN28	−4.71	−4.28	−4.56	−4.59	−4.59	−4.65	−4.56	−4.60	−6.10	−5.93	−5.68	−6.51	−6.81	−4.72	−4.89
MKN45	−4.72	−4.00	−4.51	−4.41	−4.46	−4.73	−4.41	−4.43	−6.06	−5.90	−5.69	−6.71	−6.82	−4.71	−4.87
MKN74	−4.74	−4.40	−4.61	−4.63	−4.61	−4.73	−4.68	−4.67	−5.97	−5.92	−5.61	−6.92	−7.00	−5.10	−5.42
DU-145	−4.68	−4.00	−4.25	−4.78	−4.41	−4.42	−4.44	−4.54	−6.08	−5.82	−5.75	−7.43	−7.55	−4.59	−5.02
PC-3	−4.74	−4.00	−4.58	−4.65	−4.48	−4.74	−4.39	−4.51	−5.83	−5.77	−5.61	−6.67	−6.69	−4.89	−4.74

abbreviations, applications, targets, and known mechanisms of 130 chemicals and 21 anticancer drugs. Approximately 15% of the chemicals were assessed twice or more. Approximately 40% of the chemicals tested had little effect on the growth of cells in the JFCR39 panel. However, the rest of the chemicals significantly inhibited the cell growth across the JFCR39 panel. For example, Fig. 1 shows the dose response curves of the cells in the JFCR39 panel against digoxin. The concentration at which the cell growth is inhibited by 50% represents GI50. Figure 2 shows the fingerprints of four chemicals [digoxin, ouabain, snake venom from *N. nigricollis* (SV-NN), and snake venom from *N. naja kaouthia* (SV-NNK)], which differentially inhibited the growth of cells in the JFCR39 panel; these fingerprints were drawn based on a calculation using a set of GI50s and clearly represented the GI50 pattern. These results were highly reproducible in that the Pearson correlation coefficient of the duplicate experiments for digoxin was 0.839 ($p < 0.001$) and that for ouabain was 0.864 ($p < 0.001$). It is noteworthy that, digoxin and ouabain, both of which are cardiac glycosides and inhibit Na-K ATPase, showed similar fingerprints. The fingerprints of SV-NNK and SV-NN, which belong to the elapidae, known as cobras, were also similar, but were different from the fingerprints of digoxin and ouabain. Table 2 summarizes only a portion of the GI50 values from 160 experiments involving 130 chemicals and 42 experiments involving 21 anticancer drugs. GI50 values from all experiments are described in the Supplemental Data (Table S1). All these data were stored in a chemosensitivity database and used for further analysis.

Classification of the Chemicals by Hierarchical Clustering. Sixty-nine chemicals were selected for further analysis based on the following criteria: 1) GI50 values for the test chemical can be determined for at least 10 cell lines in the JFCR39 panel, and 2) the range of log GI50 for the test chemical is more than 0.6, suggesting differential growth inhibition. We analyzed the GI50 values of these 69 chemicals and 20 anticancer drugs by hierarchical clustering analysis (Fig. 3). We found approximately 12 clusters (threshold: $r = 0$, Fig. 3, clusters A–L), which were further divided into 49 subclusters (threshold: $r = 0.408$, Fig. 3, clusters A1–L6).

Analysis of Clusters. Most anticancer drugs we have tested belonged either to cluster A or cluster H, depending on their modes of action (Dan et al., 2002). The targets of the anticancer drugs belonging to the cluster A were related to DNA (Topo I, antimetabolite of pyridine, DNA alkylator) and the target of the anticancer drugs belonging to the cluster H was tubulin. We presently found that cisplatin exceptionally belonged to cluster F2, not cluster A, although it is known to cross-link DNA strands (Jamieson and Lippard, 1999; Wong and Giandomenico, 1999). We were also able to precisely group the clusters into several subclusters having similar characteristics. For example, the cardiac glycosides digoxin and ouabain were grouped in one cluster (cluster F3). SV-

S3243	S3244	S1534	S3237	S3238	S1525	S3236	S1928	S1421	S1705	S1327	S1413	S1413	S3408	S3409	S2421
−599	−599	−270	−270	−270	−261	−261	−261	−247	−247	−232	−232	−232	−421	−421	−421
Thiram		Ziram			Paraquat			Ouabain		Digoxin			TBT		
−4	−4	−4	−4	−4	−4	−3	−4	−4	−6	−4	−4	−4	−4	−4	−4
−4.71	−4.79	−5.80	−5.73	−5.70	−4.00	−3.61	−4.00	−7.54	−7.28	−6.57	−6.96	−6.96	−6.79	−6.77	−6.72
−6.97	−7.12	−6.85	−6.76	−6.60	−4.00	−4.45	−4.51	−8.00	−7.76	−7.58	−7.68	−7.68	−7.03	−7.01	−6.83
−7.41	−7.66	−7.18	−7.47	−7.47	−4.68	−4.70		−7.76	−7.51	−7.15	−7.44	−7.44	−6.76	−6.88	−6.83
−4.77	−4.80	−6.00	−5.84	−5.83	−4.06	−3.72	−4.00	−7.64	−7.51	−7.29	−7.39	−7.39	−6.86	−6.84	−6.79
−4.66	−4.68	−5.64	−5.75	−5.63	−4.00	−3.57	−4.00	−7.40	−6.81	−6.41	−6.72	−6.72	−6.83	−6.81	−6.70
−4.75	−4.78	−5.71	−5.79	−5.82	−4.00	−3.69	−4.00	−7.75	−7.16	−7.01	−7.40	−7.40	−6.79	−6.77	−6.72
−4.86	−4.96	−5.74	−5.83	−7.01	−4.00	−4.08	−4.00	−8.00	−7.77	−7.42	−7.70	−7.70	−6.84	−6.85	−6.71
−4.77	−4.89	−5.71	−5.70	−5.79	−4.47	−4.37	−4.20	−8.00	−7.64	−7.42	−7.55	−7.55	−6.75	−6.73	−6.76
−4.75	−4.88	−5.73	−5.75	−5.77	−4.00	−4.03	−4.00	−8.00	−7.70	−7.46	−7.63	−7.63	−6.77	−6.72	−6.67
−4.71	−4.96	−5.79	−5.92	−5.80	−4.00	−3.94	−4.00	−7.70	−7.45	−6.86	−7.40	−7.40	−6.99	−6.95	−7.05
−4.70	−4.78	−5.69	−5.64	−5.69	−4.00	−3.78	−4.00	−7.98	−7.64	−7.45	−7.60	−7.60	−6.72	−6.79	−6.70
−4.82	−4.69	−5.76	−5.79	−5.81	−4.00	−3.70	−4.00	−7.64	−6.77	−6.68	−7.25	−7.25	−6.77	−6.79	−6.72
−4.80	−4.80	−5.43	−5.74	−5.73	−4.00	−3.58	−4.00	−7.67	−7.12	−6.69	−7.34	−7.34	−7.00	−6.98	−6.74
−4.68	−4.85	−5.75	−5.77	−5.76	−4.10	−4.03	−4.07	−7.75	−7.31	−7.20	−7.34	−7.34	−6.89	−6.84	−6.66
−4.68	−4.75	−5.70	−5.72	−5.83	−4.00	−3.64	−4.00	−7.74	−7.63	−6.92	−7.54	−7.54	−6.88	−6.84	−6.70
−4.72	−4.72	−5.74	−5.68	−5.77	−4.00	−3.60	−4.00	−8.00	−7.57	−7.47	−7.62	−7.62	−6.90	−6.85	−6.74
−4.69	−4.78	−5.96	−5.85	−5.84	−4.19	−4.18	−4.00	−8.00	−7.67	−7.50	−7.84	−7.84	−6.90	−6.85	−6.76
−6.33	−6.74	−5.63	−5.96	−6.12	−4.41	−4.41	−4.00	−8.00	−7.37	−6.93	−7.61	−7.61	−6.99	−6.91	−6.74
−7.49	−7.50	−7.44	−7.66	−8.00	−4.49	−4.71	−4.59	−8.00	−7.64	−7.59	−7.91	−7.91	−6.83	−6.80	−6.25
−6.14	−6.16	−6.30	−6.10	−6.15	−4.30	−4.45	−4.37	−8.00	−7.74	−7.60	−7.77	−7.77	−6.98	6.98	−6.56
−4.84	−4.82	−5.97	−5.91	−5.91	−4.49	−4.49	−4.41	−8.00	−7.80	−7.66	−7.91	−7.91	−6.82	−6.87	−6.73
−6.64	−6.58	−6.43	−6.84	−6.82	−4.25	−4.43	−4.30	−8.00	−7.71	−7.48	−7.72	−7.72	−6.74	−6.75	−6.70
−7.18	−7.39	−7.37	−7.38	−7.43	−4.50	−4.63	−4.27	−8.00	−7.84	−7.73	−8.00	−8.00	−7.11	−7.12	−7.02
−4.68	−4.71	−5.66	−5.71	−5.70	−4.00	−3.51	−4.00	−7.80	−7.80	−7.39	−7.46	−7.46	−6.93	−6.94	−6.76
−4.86	−6.25	−6.07	−6.35	−6.32	−4.00	−4.46	−4.28	−8.00	−7.66	−7.64	−7.59	−7.59	−6.80	−6.82	−6.74
−4.77	−6.67	−5.90	−5.91	−5.87	−4.00	−4.21	−4.48	−8.00	−7.71	−7.71	−7.72	−7.72	−6.91	−7.20	−6.80
−4.90	−6.00	−6.11	−6.91	−6.74	−4.00	−3.98	−4.00	−7.89	−7.62	−7.12	−7.42	−7.42	−6.90	−6.93	−6.75
−4.62	−4.74	−5.59	−5.68	−5.67	−4.00	−3.84	−4.00	−7.85	−7.44	−6.97	−7.29	−7.29	−6.73	−6.67	−6.57
−4.39	−4.38	−4.92	−5.49	−5.53	−4.00	−3.39	−4.00	−7.74	−7.67	−7.18	−7.38	−7.38	−6.80	−6.77	−6.68
−4.75	−4.65	−5.57	−5.63	−5.60	−4.00	−3.60	−4.00	−7.10	−6.00	−6.42	−6.20	−6.20	−6.78	−6.76	−6.68
−4.52	−4.60	−5.64	−5.68	−5.69	−4.00	−3.51	−4.00	−8.00	−7.72	−7.44	−7.59	−7.59	−6.78	−6.77	−6.76
−4.59	−4.72	−5.99	−5.73	−5.81	−4.00	−3.58	−4.00	−8.00	−7.65	−7.45	−7.60	−7.60	−6.80	−6.80	−6.72
−4.80	−4.85	−6.82	−5.84	−5.92	−4.41	−4.61	−4.48	−8.00	−7.72	−7.68	−7.72	−7.72	−7.25	−7.15	−6.87
−4.79	−4.82	−6.56	−5.84	−5.82	−4.08	−4.29	−4.32	−7.80	−7.48	−6.98	−7.47	−7.47	−7.34	−7.07	−6.86
−7.18	−7.21	−5.82	−7.09	−7.13	−4.00	−4.40	−4.18	−7.70	−7.42	−6.77	−7.37	−7.37	−6.84	−6.82	−6.87
−6.65	−6.71	−6.05	−7.18	−6.86	−4.00	−4.29	−4.35	−7.77	−7.25	−6.99	−7.52	−7.52	−6.96	−6.97	−6.87
−7.05	−7.08	−6.35	−5.86	−7.05	−4.00	−4.47	−4.06	−7.91	−7.65	−7.55	−7.74	−7.74	−6.97	−7.37	−7.05
−4.47	−4.70	−5.68	−5.68	−5.65	−4.00	−3.57	−4.00	−8.00	−7.64	−7.59	−7.71	−7.71	−6.90	−6.89	−6.70
−4.42	−4.77	−5.61	−5.53	−5.56	−4.00	−3.64	−4.37	−8.00	−7.62	−7.41	−7.62	−7.62	−6.77	−6.78	−6.73

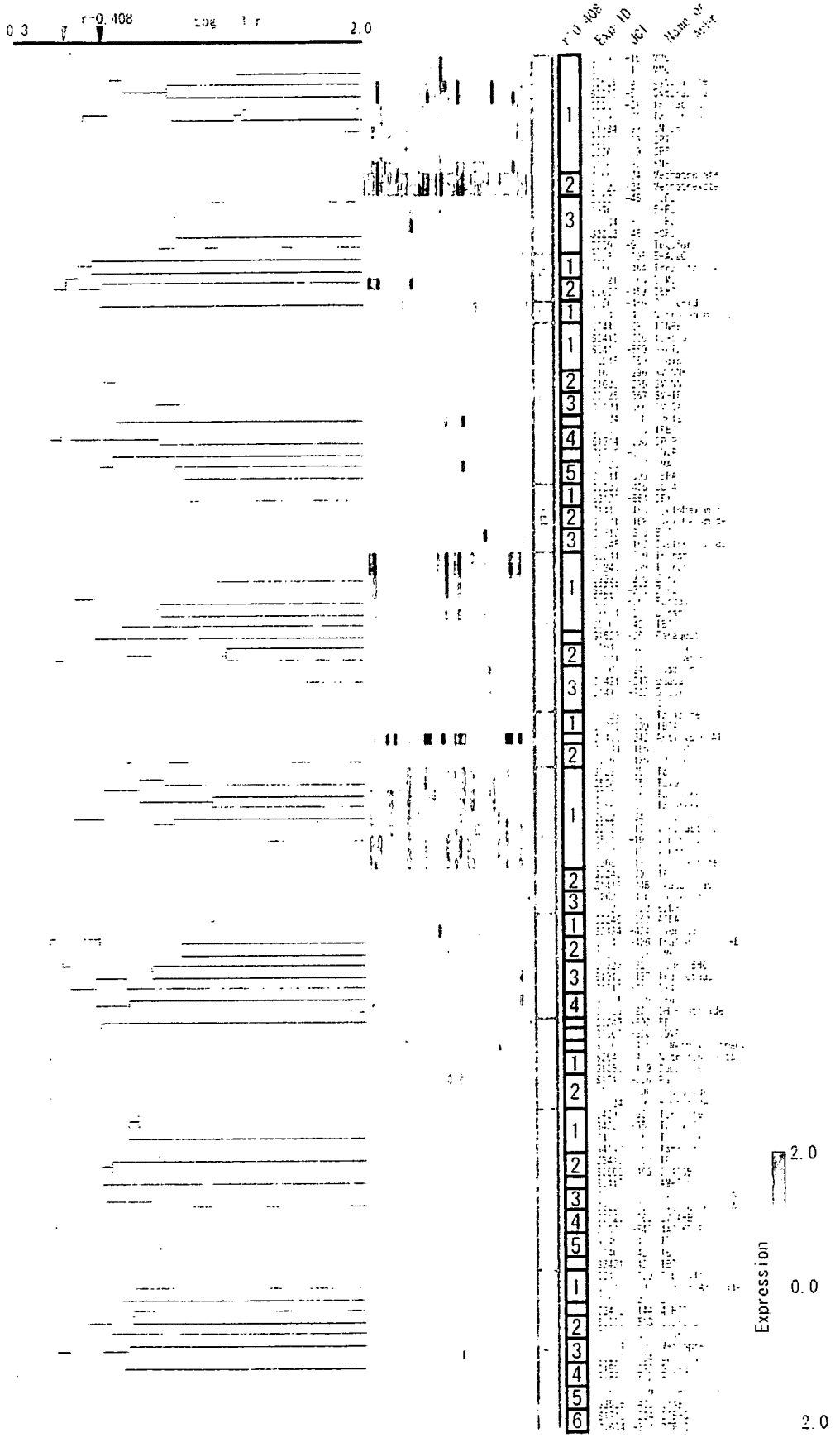

Fig. 3. Hierarchical clustering of 69 test chemicals and 20 anticancer drugs based on their GI50 values. Hierarchical clustering method was an "average linkage method" using the Pearson correlation as distance. We classified the chemicals into two kinds of clusters; their threshold values were $r = 0$ and $r = 0.408$ ($p < 0.01$), respectively. Gradient color indicates relative level (log transformed) of GI50. Red, more sensitive than the mean GI50 (2.0); yellow, mean GI50 (0.0); and green, less sensitive than the mean GI50 (−2.0). On the color scale, red represents the GI50 value that is 100-fold higher than the mean GI50.

NNK and SV-NN, on the other hand, belonged to the cluster D2. These results are in accordance with the similar fingerprints shown in Fig. 2. It is noteworthy that the snake venoms from the *C. atrox* and *T. flavoviridis*, species belonging to the viperidae family of snakes, formed another cluster (cluster D3), which was different from that of the elapidae family of snakes, *N. naja kaouthia* and *N. nigricollis*. 9-*cis* Retinoic acid, 13-*cis* retinoic acid, and 4-[*E*-2-(5,6,7,8-tetrahydro-5,5,8,8-tetra-methyl-2-naphthalenyl)-1-propenyl]benzoic acid, which are RAR agonists (Aström et al., 1990), also formed a separate cluster (cluster D1). Likewise, agricultural chemicals paraquat, ziram, and thiram formed a single cluster (cluster F1).

Discussion

The JFCR39 system coupled to a drug activity database is a good model for investigating the diversity of chemosensitivity in cancer cells. We have previously established panels of human cancer cell lines [JFCR39 (Yamori, 2003) and JFCR45 (Nakatsu et al., 2005)]. We used these panels of cells to demonstrate that they provide powerful means to predict the action mechanisms of drugs, and also used them to identify new target compounds. In this manuscript, we used the JFCR39 system to evaluate various chemicals (such as toxic chemicals, agricultural chemicals, and synthetic intermediates), which are not anticancer drugs, and classified them according to their molecular target or action mechanism. As a result, these chemicals were classified into a number of clusters. Our results also suggested that each cluster consisted of chemicals sharing a common action mechanism.

We determined the growth inhibition of cells in the JFCR39 panel by 130 chemicals and calculated their GI50 values. Some of the chemicals were assessed twice or more to confirm the reproducibility of the assay. We had to exclude 61 chemicals from further analysis because they did not inhibit the cells in the JFCR39 panel significantly. The rest of the chemicals (69 of 130, ~60%) met our selection criteria and were evaluated by cluster analysis.

First, we found that the chemicals tested in duplicate formed tight clusters, showing high reproducibility. Next, we investigated the difference between these 69 test chemicals and the anticancer drugs. Sixty-nine chemicals, which are not anticancer drugs, formed several clusters, which were different from the anticancer drug clusters. These results suggest that the action mechanisms of these chemicals are different from the action mechanisms of the anticancer drugs. However, we found that cisplatin did not belong to the cluster A, which consisted of DNA-targeting anticancer drugs. We do not understand the reason at present. However, there is a possibility that cisplatin has other action mechanisms, which may have made the fingerprint of cisplatin different from those of other DNA-targeting drugs. Indeed, cisplatin is known to form DNA-protein cross-links (Zwelling et al., 1979; Chválová et al., 2007).

Our analysis also identified several interesting clusters. For example, the cluster F3 consisted of cardiac glycosides digoxin and ouabain, both of which inhibit Na-K ATPase (Reuter et al., 2002). The cluster D1 consisted of 9-*cis* retinoic acid, 13-*cis* retinoic acid, and 4-[*E*-2-(5,6,7,8-tetrahydro-5,5,8,8-tetra-methyl-2-naphthalenyl)-1-propenyl]benzoic acid, which are RAR agonists. These results suggest that chemicals other than the anticancer drugs also form clusters when they share the same action mechanisms. It is noteworthy that SV-NNK and SV-NN, from snakes that belonged to the elapidae family, formed one cluster (cluster D2). In contrast, the snake venoms from the *C. atrox* and *T. flavoviridis*, which belonged to the viperidae family, formed a cluster (cluster D3) different from the elapidae cluster. These results are reasonable because snake venoms from different snake families are known to differ not only in composition but also in levels of toxicity and mechanisms of action.

The agricultural chemicals paraquat, ziram, and thiram were also classified into a single cluster (cluster F1). Among these agricultural chemicals, the action mechanism of ziram is not known. However, both paraquat and thiram are known to induce oxidative stress (Cereser et al., 2001; Suntres, 2002). Therefore, based on our observations, we could suggest that ziram also acted by inducing oxidative stress. The agricultural chemicals methoprene (insect growth regulator) and carbaryl (chorine esterase inhibitor) formed cluster L3, although their common mechanism is unknown. Cluster D4 and D5 consist of the antibacterial agents or fungicides. 3-Iodo-2-propynyl-butylcarbamate and *p*-chlorophenyl-3′-iodopropargylformal, belonging to cluster D4, are the iodo-type antibacterial agents.

Thus, cluster analysis of GI50 values of various chemicals, determined using the JFCR39 cell panel, suggests that the JFCR39 system could, at least in part, allow classification of chemical compounds on the basis of their action mechanisms. Our analysis also suggests that the chemicals belonging the same cluster share a common action mechanism. We are going to develop a larger library of reference chemicals with known action mechanisms (i.e., various inhibitors of biological pathways), and expand our database by integrating their GI50 measurements, which will make the cluster analysis as well as the COMPARE analysis more informative for predicting the mechanism of test chemicals.

In conclusion, to evaluate the potential of the JFCR39 system in predicting the action mechanisms of toxic chemicals, we investigated the fingerprints of 130 different types of chemical compounds including toxic chemicals, pesticides, drugs, and synthetic intermediates. Using the hierarchical clustering analysis, we classified 69 chemicals, at least in part, based on their action mechanisms. Thus, this approach using the JFCR39 cell panel is useful not only in predicting the action mechanisms of toxic chemicals but also in evaluating their toxicity.

Acknowledgments

We thank Yumiko Mukai, Yumiko Nishimura, and Mariko Seki for determination of chemosensitivity and Satoshi Kitajima for help with chemical information.

References

Akashi T, Nishimura Y, Wakatabe R, Shiwa M, and Yamori T (2007) Proteomics-based identification of biomarkers for predicting sensitivity to a PI3-kinase inhibitor in cancer. *Biochem Biophys Res Commun* **352**:514–521.

Akashi T and Yamori T (2007) A novel method for analyzing phosphoproteins using SELDI-TOF MS in combination with a series of recombinant proteins. *Proteomics* 7:2350–2354

Aström A, Pettersson U, Krust A, Chambon P, and Voorhees JJ (1990) Retinoic acid and synthetic analogs differentially activate retinoic acid receptor dependent transcription. *Biochem Biophys Res Commun* **173**:339–345.

Cereser C, Boget S, Parvaz P, and Revol A (2001) An evaluation of thiram toxicity on cultured human skin fibroblasts. *Toxicology* **162**:89–101.

Chválová K, Brabec V, and Kasparkova J (2007) Mechanism of the formation of DNA-protein cross-links by antitumor cisplatin. *Nucleic Acids Res* **35**:1812–1821.

Dan S, Shirakawa M, Mukai Y, Yoshida Y, Yamazaki K, Kawaguchi T, Matsuura M, Nakamura Y, and Yamori T (2003) Identification of candidate predictive markers of anticancer drug sensitivity using a panel of human cancer cell lines. *Cancer Sci* **94**:1074–1082.

Dan S, Tsunoda T, Kitahara O, Yanagawa R, Zembutsu H, Katagiri T, Yamazaki K, Nakamura Y, and Yamori T (2002) An integrated database of chemosensitivity to 55 anticancer drugs and gene expression profiles of 39 human cancer cell lines. *Cancer Res* **62**:1139–1147.

Hershberger LG, Shipley EG, and Meyer RK (1953) Myotrophic activity of 19-nortestosterone and other steroids determined by modified levator ani muscle method. *Proc Soc Exp Biol Med* **83**:175–180.

Jamieson ER and Lippard SJ (1999) Structure, Recognition, and Processing of Cisplatin-DNA Adducts. *Chem Rev* **99**:2467–2498.

Kanno J, Kato H, Iwata T, and Inoue T (2002) Phytoestrogen-low diet for endocrine disruptor studies. *J Agric Food Chem* **50**:3883–3885.

Naasani I, Seimiya H, Yamori T, and Tsuruo T (1999) FJ5002: a potent telomerase inhibitor identified by exploiting the disease-oriented screening program with COMPARE analysis. *Cancer Res* **59**:4004–4011.

Nakamura H, Dan S, Akashi T, Unno M, and Yamori T (2007) Absolute quantification of four isoforms of the class I phosphoinositide-3-kinase catalytic subunit by real-time RT-PCR. *Biol Pharm Bull* **30**:1181–1184.

Nakatsu N, Yoshida Y, Yamazaki K, Nakamura T, Dan S, Fukui Y, and Yamori T (2005) Chemosensitivity profile of cancer cell lines and identification of genes determining chemosensitivity by an integrated bioinformatical approach using cDNA arrays. *Mol Cancer Ther* **4**:399–412.

Okutsu J, Tsunoda T, Kaneta Y, Katagiri T, Kitahara O, Zembutsu H, Yanagawa R, Miyawaki S, Kuriyama K, Kubota N, et al. (2002) Prediction of chemosensitivity for patients with acute myeloid leukemia, according to expression levels of 28 genes selected by genome-wide complementary DNA microarray analysis. *Mol Cancer Ther* **1**:1035–1042.

Paull KD, Shoemaker RH, Hodes L, Monks A, Scudiero DA, Rubinstein L, Plowman J, and Boyd MR (1989) Display and analysis of patterns of differential activity of drugs against human tumor cell lines: development of mean graph and COMPARE algorithm. *J Natl Cancer Inst* **81**:1088–1092.

Reuter H, Henderson SA, Han T, Ross RS, Goldhaber JI, and Philipson KD (2002) The Na^+–Ca^{2+} exchanger is essential for the action of cardiac glycosides. *Circ Res* **90**:305–308.

Scherf U, Ross DT, Waltham M, Smith LH, Lee JK, Tanabe L, Kohn KW, Reinhold WC, Myers TG, Andrews DT, et al. (2000) A gene expression database for the molecular pharmacology of cancer. *Nat Genet* **24**:236–244.

Suntres ZE (2002) Role of antioxidants in paraquat toxicity. *Toxicology* **180**:65–77.

Weinstein JN, Kohn KW, Grever MR, Viswanadhan VN, Rubinstein LV, Monks AP, Scudiero DA, Welch L, Koutsoukos AD, and Chiausa AJ (1992) Neural computing in cancer drug development: predicting mechanism of action. *Science* **258**:447–451.

Weinstein JN, Myers TG, O'Connor PM, Friend SH, Fornace AJ Jr, Kohn KW, Fojo T, Bates SE, Rubinstein LV, Anderson NL, et al. (1997) An information-intensive approach to the molecular pharmacology of cancer. *Science* **275**:343–349.

Wong E and Giandomenico CM (1999) Current status of platinum-based antitumor drugs. *Chem Rev* **99**:2451–2466.

Yaguchi S, Fukui Y, Koshimizu I, Matsuno T, Gouda H, Hirono S, Yamazaki K, and Yamori T (2006) Antitumor activity of ZSTK474, a new phosphatidyl inositol 3-kinase inhibitor. *J Natl Cancer Inst* **98**:545–556.

Yamori T (2003) Panel of human cancer cell lines provides valuable database for drug discovery and bioinformatics. *Cancer Chemother Pharmacol* **52 (Suppl 1)**: S74–S79

Yamori T, Matsunaga A, Sato S, Yamazaki K, Komi A, Ishizu K, Mita I, Edatsugi H, Matsuba Y, Takezawa K, et al. (1999) Potent antitumor activity of MS-247, a novel DNA minor groove binder, evaluated by an in vitro and in vivo human cancer cell line panel. *Cancer Res* **59**:4042–4049.

Zembutsu H, Ohnishi Y, Tsunoda T, Furukawa Y, Katagiri T, Ueyama Y, Tamaoki N, Nomura T, Kitahara O, Yanagawa R, et al. (2002) Genome-wide cDNA microarray screening to correlate gene expression profiles with sensitivity of 85 human cancer xenografts to anticancer drugs. *Cancer Res* **62**:518–527.

Zwelling LA, Anderson T, and Kohn KW (1979) DNA-protein and DNA interstrand cross-linking by cis- and trans-platinum(II) diamminedichloride in L1210 mouse leukemia cells and relation to cytotoxicity. *Cancer Res* **39**:365–369.

Address correspondence to: Takao Yamori, Division of Molecular Pharmacology, Cancer Chemotherapy Center, Japanese Foundation for Cancer Research, 3-10-6, Ariake, Koto-ku, Tokyo 135-8550, Japan. E-mail: yamori@jfcr.or.jp. 07a$sl

Periostin is essential for cardiac healing after acute myocardial infarction

Masashi Shimazaki,[1] Kazuto Nakamura,[2] Isao Kii,[1] Takeshi Kashima,[3] Norio Amizuka,[4] Minqi Li,[4] Mitsuru Saito,[5] Keiichi Fukuda,[6] Takashi Nishiyama,[1] Satoshi Kitajima,[7] Yumiko Saga,[8] Masashi Fukayama,[3] Masataka Sata,[2] and Akira Kudo[1]

[1]Department of Biological Information, Tokyo Institute of Technology, Yokohama 226-8501, Japan
[2]Department of Cardiovascular Medicine and [3]Department of Pathology, Graduate School of Medicine, The University of Tokyo, Tokyo 113-0033, Japan
[4]Center for Transdisciplinary Research, Niigata University, Niigata 951-8514, Japan
[5]Department of Orthopaedic Surgery, Jikei University School of Medicine, Tokyo 105-8461, Japan
[6]Department of Regenerative Medicine and Advanced Cardiac Therapeutics, Keio University School of Medicine, Tokyo 160-8582, Japan
[7]Division of Cellular and Molecular Toxicology, National Institute of Health Science, Tokyo 158-8501, Japan
[8]Division of Mammalian Development, National Institute of Genetics, Mishima 411-8540, Japan

Acute myocardial infarction (AMI) is a common and lethal heart disease, and the recruitment of fibroblastic cells to the infarct region is essential for the cardiac healing process. Although stiffness of the extracellular matrix in the infarct myocardium is associated with cardiac healing, the molecular mechanism of cardiac healing is not fully understood. We show that periostin, which is a matricellular protein, is important for the cardiac healing process after AMI. The expression of periostin protein was abundant in the infarct border of human and mouse hearts with AMI. We generated *periostin*$^{-/-}$ mice and found no morphologically abnormal cardiomyocyte phenotypes; however, after AMI, cardiac healing was impaired in these mice, resulting in cardiac rupture as a consequence of reduced myocardial stiffness caused by a reduced number of α smooth muscle actin–positive cells, impaired collagen fibril formation, and decreased phosphorylation of FAK. These phenotypes were rescued by gene transfer of a spliced form of periostin. Moreover, the inhibition of FAK or αv-integrin, which blocked the periostin-promoted cell migration, revealed that αv-integrin, FAK, and Akt are involved in periostin signaling. Our novel findings show the effects of periostin on recruitment of activated fibroblasts through FAK-integrin signaling and on their collagen fibril formation specific to healing after AMI.

CORRESPONDENCE
Akira Kudo:
akudo@bio.titech.ac.jp

Periostin, which is an extracellular matrix (ECM) molecule of the fasciclin family, acts in cell adhesion, migration, and growth in vitro (1–6). In the heart, periostin is expressed at very early stages of embryogenesis; however, it is not detected in the normal adult myocardium, except in the valves (7, 8) and in the case of various heart diseases (9–12).

The early cardiac healing process after acute myocardial infarction (AMI) can be divided into two successive phases: the inflammatory phase and the scar formation phase. In the inflammatory phase, monocytes and lymphocytes infiltrate into the necrotic myocardium, whereas in the scar formation phase, activated interstitial or circulating fibroblasts increase their motility and migrate into the lesion. The activation of TGFβ is important for regulation of this latter process. Myofibroblasts expressing α smooth muscle actin (αSMA) induced by TGFβ are specialized fibroblasts that share characteristics with smooth muscle cells (SMCs). They play an important role in wound healing by synthesizing ECM and exerting strong contraction forces to minimize wound areas (13–16). Regarding the inflammatory phase, recent knockout mouse studies indicated a positive association of inflammatory factors with cardiac rupture or dilation (17–23). However, in the scar formation phase, molecular analysis has been scant, except in respect to TGFβ. To answer two important questions for both cardiologists and basic scientists who are interested in pathological myocardial healing, i.e., "what regulates formation of

The online version of this article contains supplemental material.

JEM © The Rockefeller University Press $30.00
Vol. 205, No. 2, February 18, 2008 295–303 www.jem.org/cgi/doi/10.1084/jem.20071297

Supplemental Material can be found at:
http://www.jem.org/cgi/content/full/jem.20071297/DC1

the scar phase of an ischemic injury?" and "what is the nature of the factors responsible for the ventricular healing process after AMI?," we focused on periostin, which is a TGFβ-responding factor (1).

RESULTS AND DISCUSSION

To assess the importance of periostin in the cardiac healing process, we examined the expression of human periostin protein in the myocardial tissue of the left ventricle (LV). No expression of it was observed in the normal myocardium (Fig. 1 A), whereas immunoreactivity indicating periostin was detected in Azan-stained myocardial fibrous areas from a patient with AMI (Fig. 1, B and C), thus suggesting that periostin expression was induced in the infarct regions after AMI. In the fibrous area, strong immunoreactivity of periostin was observed around cardiac fibroblasts expressing αv-integrin, which is reported to be a receptor for periostin (Fig. 1 C) (2, 6). Next, we examined the expression of periostin in mice after AMI caused by left anterior descending artery (LAD) ligation (24). Periostin protein was not observed up to day 2, but became detectable at day 3 in the areas showing inflammatory infiltration (Fig. 1 D). This expression in the infarct LV increased significantly at day 4, and was still present at day 28 (Fig. 1 D and not depicted). To identify the cells producing periostin, we performed RNA in situ hybridization to detect *periostin* mRNA in the infarct LV wall of mice. *Periostin* mRNA was mainly expressed in fibroblasts in both the infarct and noninfarct regions after AMI (Fig. 1 E). To confirm the periostin expression in cardiac fibroblasts, we performed RT-PCR analysis on purified cardiac cells, and these results showed the expression to be mainly in cardiac fibroblasts, but not in cardiomyocytes (Fig. S1, available at http://www.jem.org/cgi/content/full/jem.20071297/DC1). Furthermore, these fibroblasts were positive for αv-integrin, as indicated by flow cytometry using cultured cardiac cells (Fig. S1). The mRNA of *βig-h3*, another fascidin family member, which is also expressed in the embryonic heart (25), was not observed in

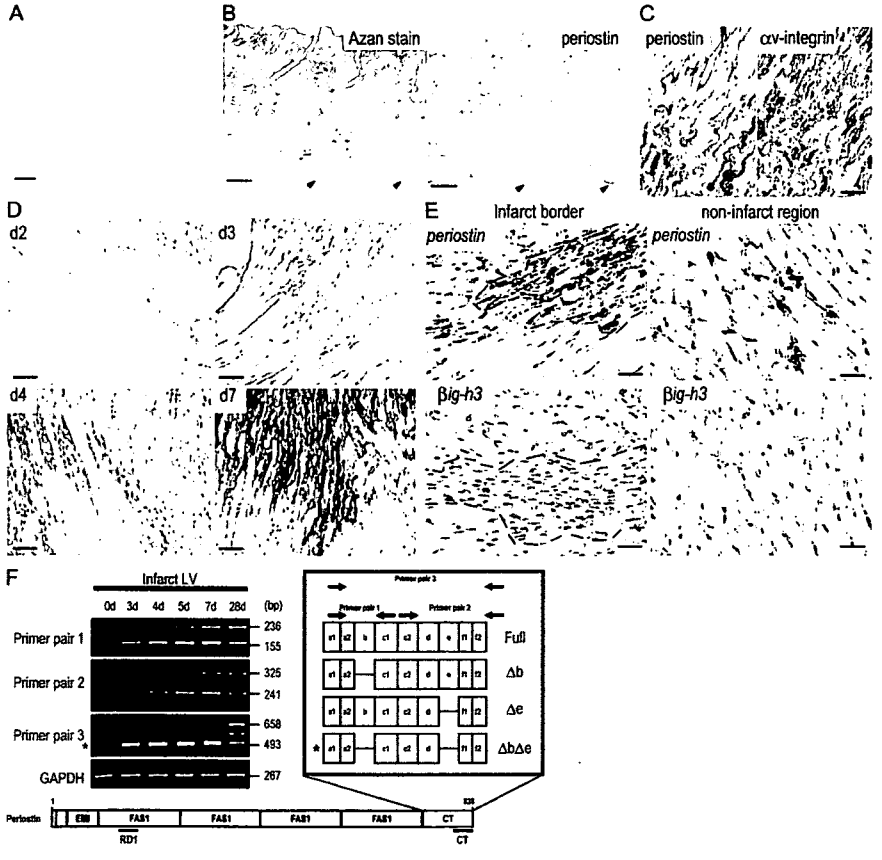

Figure 1. Periostin expression is induced after myocardial ischemia. (A–C) Detection of periostin in myocardium from human patients. LV tissue from a patient with alcoholic cirrhosis (A) and from a patient with AMI (B and C). As seen by immunostaining, periostin protein was detected (B, right) in the myocardial area, which was shown to be fibrous by Azan staining (B, left). Arrowheads in B indicate endocardium. (C) Comparison of the expression pattern between periostin (left) and αv-integrin (right) in the fibrous area. (D–F) Periostin is up-regulated after AMI in mice. (D) Immunostaining of periostin after AMI. (E) Expression of *periostin* (top) and β *ig-h3* mRNA (bottom) in the infarct LV wall of mice was analyzed by in situ hybridization. The dashed red line shows the infarct border. (F) Expression of spliced variant forms of periostin at various times after AMI. Periostin ΔbΔe is indicated by the asterisk. Bars: (A) 25 μm; (B) 2 mm; (C–E) 50 μm.

the same regions (Fig. 1 E), thus suggesting the AMI-induced expression of fasciclin family molecules to be specific to periostin.

Because we previously reported that several *periostin* transcripts exist in human and mouse, caused by alternative splicing at a 3′ site (1), we examined the expression of the splice variants in a time course experiment by RT-PCR analysis using three combinations of specific primers (Fig. 1 F). We observed four different isoforms, i.e., Δb (deletion of b domain), Δe (deletion of e domain), ΔbΔe (deletion of b and e domains), and Full (full-length), and we found that the pattern of splicing depended on the time after AMI. Interestingly, one specific spliced form, ΔbΔe (Fig. 1 F, asterisk), was dominantly found as the lowest electrophoretic band in the initial stages (3, 4, and 5 d after AMI), indicating the involvement of ΔbΔe periostin in the early healing stage of damaged tissues. By 28 d, all 4 isoforms were equally expressed. We also confirmed the expression of these isoforms at the protein level, and found the proteolytic modification of periostin during infarct healing (Fig. S1).

To investigate the role of periostin in AMI, we generated *periostin*$^{-/-}$ mice combined with Cre recombination (Fig. 2 A and Fig. S2, available at http://www.jem.org/cgi/content/full/jem.20071297/DC1). The embryogenesis of *periostin*$^{-/-}$ mice was apparently normal; and after the birth, the mice appeared to be healthy. The observation of periostin in the developing heart prompted us to thoroughly investigate the heart structure and function in the *periostin*$^{-/-}$ mice; however, no cardiomyocyte abnormalities were found in the myocardium, valve function, pulsation, or blood pressure in the 10-wk-old mice (Fig. S2 and not depicted), which is consistent with no significant expression in the adult myocardium. We then subjected *periostin*$^{-/-}$ mice to AMI by LAD ligation. There was no significant difference in body weight or heart rate among $^{-/-}$, $^{+/-}$, and $^{+/+}$ in the normal control condition or after the AMI (Fig. S2, Table S1, and not depicted); moreover, there was no difference in infarct size between the *periostin*$^{+/+}$ and $^{-/-}$ mice after AMI (Table S1). However, the survival rate of *periostin*$^{-/-}$ mice after AMI was significantly lower than that of $^{+/+}$ mice (17.58 vs. 53.76% at day 10; $P < 0.0001$; Fig. 2 B), whereas this rate of *periostin*$^{+/-}$ mice (55%) after AMI was similar to that of $^{+/+}$ mice. The incidence of mortality in *periostin*$^{-/-}$ mice, mainly caused by cardiac rupture, which occurred within 7 d, was significantly higher ($P < 0.001$) than that of $^{+/+}$ mice: 62/91 (68.1%) in $^{-/-}$ versus 25/80 (31.3%) in $^{+/+}$ (Fig. 3 C), whereas this frequency of $^{+/-}$ mice 6/20 (30%) was similar to that of $^{+/+}$ mice. Thereafter, these survival rates reached a plateau from 8 d up to 4 wk after AMI (unpublished data). To test whether the increased rate of cardiac rupture was caused by abnormal LV wall stiffness, we analyzed the rupture threshold stiffness of the LVs of *periostin*$^{-/-}$ and $^{+/+}$ mice 4 d after AMI by conducting an LV distending pressure/rupture threshold study (18). Myocardial tearing was found at the infarct border in all the ruptured LVs, and the mean of the maximum rupture pressure was significantly lower in *periostin*$^{-/-}$ mice than in $^{+/+}$ mice after AMI (312.7 ± 3.2 mmHg in $^{-/-}$ vs. 374.3 ± 5.8 mmHg in $^{+/+}$; $P = 0.0008$; $n = 5$), and the mean passive stiffness was also significantly lower in $^{-/-}$ mice than in $^{+/+}$ mice after AMI (50.26 ± 2.13 mmHg/100 μl in $^{-/-}$ vs. 65.08 ± 2.55 mmHg/100 μl in $^{+/+}$; $P = 0.001$; $n = 5$; Fig. 2 C). In contrast, no significant difference was observed between $^{+/+}$ control noninfarct mice and *periostin*$^{-/-}$ control noninfarct mice (maximum rupture pressure was 544.0 ± 6.93 mmHg in $^{-/-}$ vs. 552.7 ± 7.86 mmHg in $^{+/+}$; $P = 0.4546$; $n = 5$; mean passive stiffness was 87.07 ± 4.41 mmHg/100 μl in $^{-/-}$ vs. 88.85 ± 3.14 mmHg/100 μl in $^{+/+}$; $P = 0.5985$; $n = 5$). These biomechanical data indicate that both rupture threshold and passive stiffness in the LV of the *periostin*$^{-/-}$ infarcted mice were significantly lower than those of the $^{+/+}$ mice after AMI, suggesting that the *periostin*$^{-/-}$ infarct LV wall was more susceptible to cardiac rupture by mechanical stress. Although periostin deficiency did not affect heart structure, the circulatory system, or cardiac performance under physiological conditions, periostin induced in the infarct myocardium appears to play a pivotal role in the healing process after AMI.

To confirm the histomorphological stiffness of the wall in *periostin*$^{-/-}$ mice just escaping from rupture, we performed echocardiography 7 d after AMI, in addition to 1 d for heart tissue evaluation and 28 d for the analysis of chronic cardiac pathophysiology after AMI (Fig. 2 D and Table S1). Echocardiographic measurements made 7 d after AMI showed decreases in left ventricular end-diastolic dimension (LVEDD) and left ventricular end-systolic dimension (LVESD) in *periostin*$^{-/-}$ mice ($n = 10$), as compared with these parameters for $^{+/+}$ mice ($n = 15$; LVEDD and LVESD values for $^{-/-}$ were 89.0 and 84.4%, respectively, of those for $^{+/+}$). These results demonstrate that the absence of periostin attenuated ventricular remodeling after AMI. To further examine tissue stiffness histologically, we performed toluidine blue staining, immunofluorescence analysis using anti–collagen I, -fibronectin, and -vimentin antibodies, and transmission electron microscopic (TEM) observation of sections prepared from *periostin*$^{+/+}$ and $^{-/-}$ mice 5 d after AMI. The results showed a lower number of cardiac fibroblasts, along with sparser pericellular ECM density in the *periostin*$^{-/-}$ mice than in the $^{+/+}$ mice (Fig. 2, E and F); indeed, the number of vimentin-positive cardiac fibroblasts was decreased in the infarct region of *periostin*$^{-/-}$ mice 5 d after AMI (7,655 ± 148 cells/mm^2 in $^{+/+}$ vs. 6,913 ± 297 cells/mm^2 in $^{-/-}$; $n = 6$; $P < 0.02$; Fig. 2 C). Furthermore, reduced collagen I and fibronectin immunoreactivity was observed in the infarct border of the $^{-/-}$ mice (Fig. 2 F and Fig. S3, available at http://www.jem.org/cgi/content/full/jem.20071297/DC1), and the collagen fiber cross-sectional area (CSA) in the infarct border of *periostin*$^{-/-}$ mice was significantly smaller and more uniform than that of $^{+/+}$ mice 5 d after AMI (CSA of 1,014.642 ± 17.546 nm^2 for the $^{-/-}$ and 2,233.780 ± 25.731 nm^2 for the $^{+/+}$; $n = 6$; $P < 0.001$, respectively; Fig. 2 G). To confirm whether periostin deficiency affected the biochemical property of collagen after AMI, we evaluated the amount of collagen (hydroxyproline concentration, percentage of tissue dry weight) and nonreducible mature cross-links (mol pyridinoline per mol collagen) in the infarct zone 4 d after AMI. We detected a significant decrease in the collagen cross-linking in the *periostin*$^{-/-}$ mice, compared with the $^{+/+}$ mice

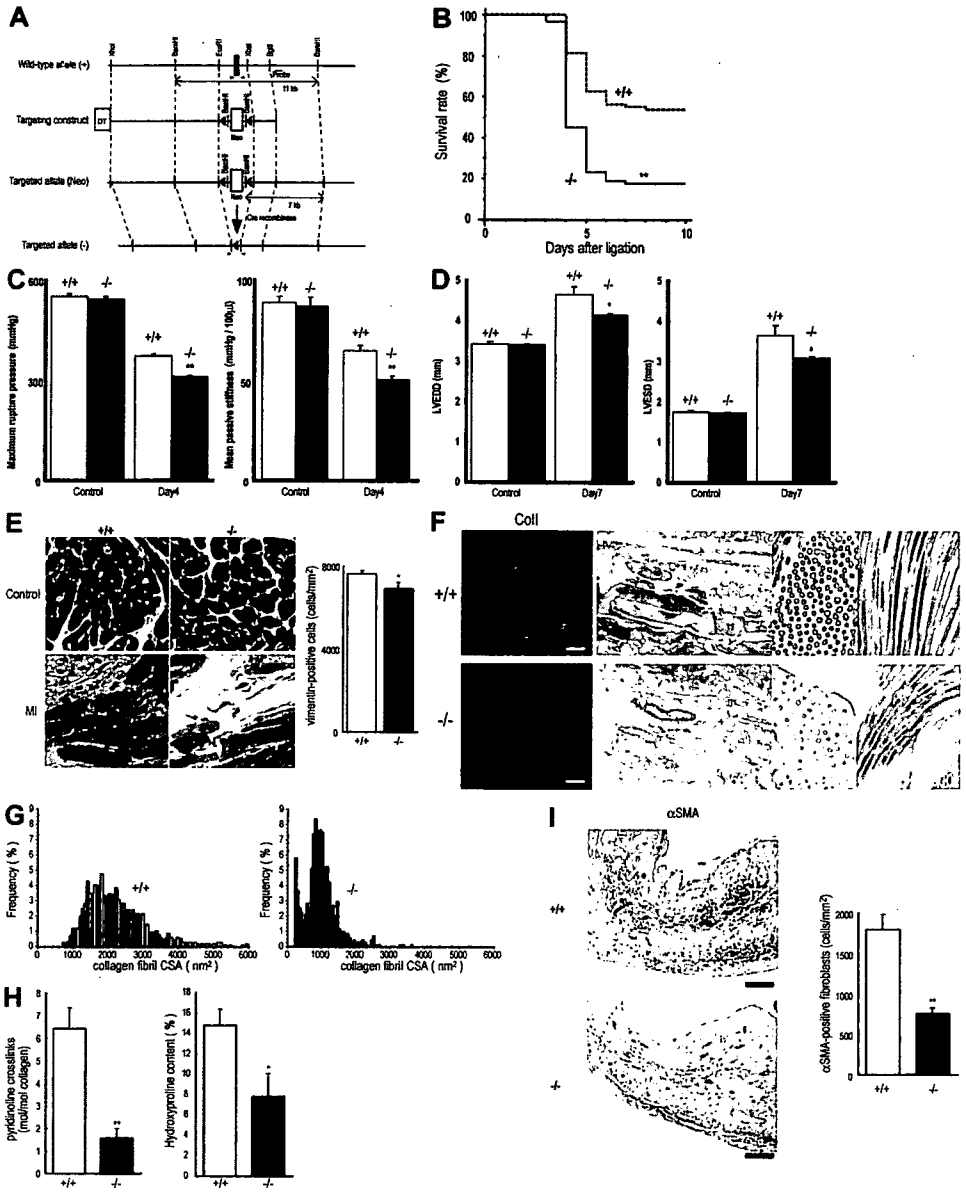

Figure 2. Cardiac rupture after AMI is caused by *periostin* disruption. (A) Schema of the targeting strategy deletes the first exon of *periostin* locus. (B) Decreased survival of *periostin*$^{-/-}$ mice (n = 91) compared with the survival of $^{+/+}$ mice (n = 80) after AMI. **, P < 0.0001. (C) Infarct LV wall stiffness was more reduced in *periostin*$^{-/-}$ mice than in $^{+/+}$ mice after AMI (left). Mean passive stiffness was also significantly lower in the $^{-/-}$ mice than in the $^{+/+}$ mice after AMI (right). Open columns, $^{+/+}$; filled columns, $^{-/-}$. **, P < 0.005, compared with $^{+/+}$ mice. (D) Loss of periostin attenuated cardiac dilation after AMI, as shown by echocardiography. Open columns, $^{+/+}$; filled columns, $^{-/-}$. *, P < 0.05 compared with $^{+/+}$ mice. (E) Histological analysis of heart sections from *periostin*$^{-/-}$ and $^{+/+}$ mice stained with toluidine blue 5 d after AMI, showing a lower number of cardiac fibroblasts and lower ECM density in $^{-/-}$ mice. (right) The number of vimentin-positive cells. *, P < 0.02, compared with $^{+/+}$ mice. (F) Images of the infarct border stained with anti-collagen I (left), and TEM images of infarct border, showing evidence of smaller and less abundant collagen in tissues from *periostin*$^{-/-}$ mice 5 d after AMI compared with the collagen of the $^{+/+}$ infarct heart. Bar, 50 μm. (G) CSA distribution of collagen fibrils in the infarct border of $^{+/+}$ and $^{-/-}$ mice, measured from TEM images. (H) Biochemical analysis of the collagen amount and cross-linking. *, P < 0.05; **, P < 0.01, compared with $^{+/+}$ mice. (I) The number of αSMA-positive cells in the infarct area was reduced in *periostin*$^{-/-}$ mice 5 d after AMI. (right) The number of αSMA-positive cells. **, P < 0.01, compared with $^{+/+}$ mice. Error bars represent the mean ± the SEM. Bars, 200 μm.

(1.555 ± 0.461 in $^{-/-}$, $n = 4$, vs. 6.433 ± 0.919 in $^{+/+}$, $n = 7$; P = 0.0043; Fig. 2 H). Moreover, the *periostin*$^{-/-}$ infarct LV tissue exhibited 52.9% less collagen content compared with the $^{+/+}$ tissue (7.832 ± 2.241% in $^{-/-}$, $n = 4$, vs. 14.795 ± 1.565% in $^{+/+}$, $n = 7$; P = 0.0283; Fig. 2 H). In normal heart tissues from mice of either genotype, the collagen amount was under the detection level by our methods (unpublished data), indicating that the detected collagen was newly produced after AMI. In conclusion, we observed the alterations of collagen structure in the *periostin*$^{-/-}$ mice; they were smaller and more uniform, with the decreased amount and cross-linking of collagen effecting lower stiffness. These results suggest that periostin expression contributed significantly to the amount or cross-linking of newly synthesized collagen, which is essential for the normal mechanical properties of collagen-containing tissues after MI. These findings indicate that impaired collagen fiber formation occurred in *periostin*$^{-/-}$ mice after AMI. Interestingly, although the total activity of myeloperoxidase and the numbers of Mac-3–positive inflammatory cells, ki67-positive proliferating cells, and active caspase-3–positive apoptotic cells in the infarct border were not significantly different between $^{+/+}$ and $^{-/-}$ mice (not depicted), we observed a lower number of αSMA-positive cells in the infarct area of *periostin*$^{-/-}$ mice 5 d after AMI (1,792 ± 193 cells/mm^2 in $^{+/+}$ vs. 758 ± 75 cells/mm^2 in $^{-/-}$; P < 0.01; $n = 6$; Fig. 2 I). However, the number of cells positive for SM1, which is a specific marker of SMCs, was not significantly different, and almost all of the αSMA-positive cells were SM1 negative (unpublished data). These results indicate that not the inflammatory cell recruitment, but rather the recruitment of cardiac fibroblasts in the infarct region, was impaired in these animals.

To determine whether the impaired cardiac healing in response to AMI could be restored by periostin directly, we performed a rescue experiment by using ΔbΔe, which is the main periostin isoform detected early after AMI. The *periostin*$^{-/-}$ mice were treated with a recombinant adenovirus expressing periostin (Ad-ΔbΔe) or with a control adenovirus (Ad-nls; nuclear localization signal-LacZ). In the control experiment, the Ad-nls-LacZ transfer was detected in the infarct border at 4 d after AMI by whole-mount X-gal staining, proving the experimental feasibility (Fig. 3 A). In *periostin*$^{-/-}$ mice infected with Ad-ΔbΔe, we first confirmed expression of transferred periostin in the infarct tissue by immunoblot and immunofluorescence analyses (Fig. 3 B and Fig. S4, available at http://www.jem.org/cgi/content/full/jem.20071297/DC1), and then observed an increase in the area reactive with anti-αSMA antibody compared with that area of the control Ad-nls-LacZ–infected *periostin*$^{-/-}$ mice (597 ± 107 cells/mm^2 in Ad-nls-LacZ–infected $^{-/-}$ mice vs. 1,535 ± 197 cells/mm^2

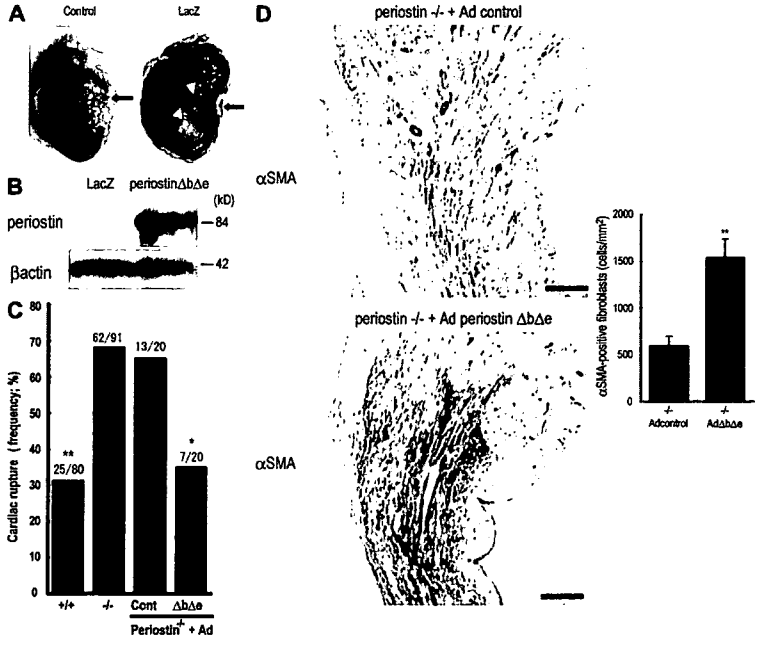

Figure 3. Adenovirus-mediated periostin ΔbΔe gene transfer prevents cardiac rupture in the *periostin*$^{-/-}$ mice. (A) Whole-mount X-gal staining 4 d after AMI showed strong expression in the border of the Ad-nls-LacZ–infected myocardial infarct (arrowheads). The arrow indicates the ligated portion. (B) Western blot analysis for Ad-ΔbΔe–infected *periostin*$^{-/-}$ infarct LV. (C) Infection with Ad-ΔbΔe reversed the high incidence of cardiac rupture in the *periostin*$^{-/-}$ mice to a lower level, comparable to the incidence in the $^{+/+}$ mice. *, P < 0.02; **, P < 0.001, compared with control Ad-treated $^{-/-}$ mice. (D) Compared with the Ad-nls-LacZ–infected *periostin*$^{-/-}$ hearts, the Ad-ΔbΔe–infected hearts increased the number of αSMA-positive cells 5 d after AMI. (right) the number of αSMA-positive cells. **, P < 0.01, compared with the mock infection of the $^{-/-}$ mice. Error bars represent the mean ± the SEM. Bars, 200 μm.